2007

Mechanics of silicon micro needle penetration in human cadaver skin and skin substitutes

Joseph E. R. P. Muthu
Lehigh University

Muthu, Joseph
E.R.P.

Mechanics of Silicon Micro Needle Penetration in Human Cadaver Skin and Skin...

May 2007

MECHANICS OF SILICON MICRO NEEDLE PENETRATION IN HUMAN CADAVER SKIN AND SKIN SUBSTITUTES

By

JOSEPH E.R.P. MUTHU

A Thesis
Presented to the Graduate and Research Committee
of Lehigh University
in Candidacy for the Degree of
Master of Science

In

Mechanical Engineering and Mechanics

Lehigh University

May 2007

THE CERTIFICATE OF APPROVAL

This thesis is accepted and approved in partial fulfillment of the requirements for the Master of Science.

25/April/07
Date

Thesis Advisor

Co-Advisor

Chairperson of Department

Acknowledgement

This project provided an excellent opportunity for me to gain experience in several exciting new areas in my field. It was an extraordinary learning experience to encounter and overcome the numerous difficulties that arise in research. I wish to extend great thanks and appreciation to my advisors, Prof. Richard P Vinci and Prof. Walter Brown for the guidance and assistance they provided to me. Thanks to Prof Anand Jagota for allowing me to use the video indentation measurement in his esteemed lab. I would also like to thank Mrs Rashmi Thakur of Rutgers University for sharing her knowledge of the handling of human cadaver skin. Lastly, I thank my parents, PichaMuthu and Victor Suseela, and all the members of my family and all my friends for their encouragement and support.

My advisors and I also wish to acknowledge the financial support of Apogee technology.

Table of Contents

Acknowledgement----------iii

Table of contents----------iv

List of tables----------vi

List of figures----------vii

Abstract----------1

1 INTRODUCTION

1.1 Motivation----------2

1.2 General Background----------2

1.3 Thesis Contribution----------4

1.4 Organization----------4

2 EXPERIMENTAL EQUIPMENT

2.1 Test Frame----------5

2.2 Needle movement----------7

2.3 Force sensor and signal conditioning----------7

2.4 Data acquisition and control----------8

2.5 Test setup Validation----------9

3 MATERIALS AND METHODS

3.1 Micro-Needle----------11

3.2 Polymers----------12

3.3 Micro Needle Mounting Procedure----------13

3.4 Skin Specimen Preparation Procedure----------14

3.5 Synthetic Polymer Specimen Preparation Procedure----------15

4 EXPERIMENTS

4.1 Human Cadaver Skin Testing----------16

4.2 Synthetic Polymer materials testing----------17

4.2.1 Synthetic Skin Model Screening Tests----------17

4.2.2 Needle Reliability tests----------18

4.3 Video Indentation----------18

4.4 Nail Polish Technique----------19

4.5 Aluminum Foil Technique----------20

5 RESULTS AND DISCUSSSION

5.1 Single needle penetration into the skin----------21

5.2 Effect of Tip Geometry----------29

5.3 Engulfment of Air gap----------32

5.4 Selection of Synthetic Skin Substitute----------35

5.5 Reliability of Silicon Micro Needles----------42

5.6 Contact Area Measurement----------46

5.7 Scaling Factor----------51

6 CONCLUSIONS

6.1 Future work----------56

References ----------57

Curriculum Vita----------59

List of tables

Table 5.1 The force and micro needle displacement of the needles when penetrated into the human cadaver skin----------27

Table 5.2 Shore A hardness values for living human skin and for a variety of elastomeric polymers----------40

Table 5.3 Measured penetration hardness and puncture force values for human cadaver skin and for a variety of elastomeric polymers------40

Table 5.4 Reliability results from normal-force testing of single needles and arrays----------43

List of Figures

Figure 2.1 Schematic diagram of the measurement system----------5

Figure 2.2 The test frame----------6

Figure 2.3 The force sensor signal conditioning units----------8

Figure 2.4 The front panel of the LabVIEW----------9

Figure 2.5 Comparisons of 50g and 1kg load cell response----------10

Figure 3.1 Pictures of the mounted micro needle----------11

Figure 3.2 Approximate correlations between durometer scales
and common materials----------12

Figure 3.3 Schematic diagram and SEM picture of constructed array----------14

Figure 3.4 Skin specimen preparations----------15

Figure 4.1 Skin mounted for testing----------17

Figure 5.1 The position of needle tip and force acting on the micro needle
when penetrated into human cadaver skin----------22

Figure 5.2 The force vs. micro needle tip advancement from the
surface of the skin----------22

Figure 5.3 The force vs. micro needle tip advancement from the surface
of the skin(magnified scale)----------24

Figure 5.4 The force vs. needle tip movement of a single needle penetrating
human cadaver skin during four successive penetrations----------25

Figure 5.5 The tests of a particular micro needle at four different
locations of skin----------26

Figure 5.6 The head on view of SEM picture of the tested micro needle----------28

Figure 5.7 The tested Skin sample----------29

Figure 5.8 A model of elastic deformation of the skin resulting in partial contact with the needle and die----------29

Figure 5.9 The head on view SEM pictures of the tested mp at high magnification----------31

Figure 5.10 The number of facets ending in a circle drawn around the tip--------32

Figure 5.11 The force vs. displacement curve during video indentation----------33

Figure 5.12 Pictures of video indentation during loading----------34

Figure 5.13 Pictures of video indentation during unloading----------34

Figure 5.14 Load –displacement curves for four tests performed at different locations in red natural latex (durometer 40A)----------35

Figure 5.15 Load –displacement curves for four tests performed at different locations in medium-hard polyurethane (durometer 60A)----------36

Figure 5.16 Load –displacement curves for four tests performed at different locations in silicone (durometer 50A)----------37

Figure 5.17 Load –displacement curves for four tests performed at different locations in silicone (durometer 20A)----------38

Figure 5.18 cone approximation of needle and area calculation----------39

Figure 5.19 Load –displacement curves for four tests performed at different locations in hard polyurethane (durometer 80A)----------42

Figure 5.20 Array 2A1A, from Lot 1 before and after testing----------45

Figure 5.21 Needles with preexisting damage before and after testing----------46

Figure 5.22 Needle tested in 20A silicone using nail polish technique----------47

Figure 5.23 Percentage height of the needle inside the material using nail polish technique----------48

Figure 5.24 optical image of the tested aluminum sheet in 20A----------49

Figure 5.25 SEM picture of the tested aluminum foil in 20A silicone----------50

Figure 5.26 The diameter of the hole vs. the depth of needle advanced using aluminum sheet technique----------50

Figure 5.27 the two curves of a 1x3 array and one curve of 3x3 array for comparison in logarithmic scale before scaling----------52

Figure 2.28 the two curves of a 1x3 array and one curve of 3x3 array for comparison in logarithmic scale after scaling----------53

Figure 5.29 needle ratio vs. the experimental ratio of different arrays compared----------54

Abstract

Silicon micro needles have been considered as a possible way to transport drug molecules through the skin with painless penetration. This thesis discusses experiments that were done to understand the mechanics of the penetration of 600 um long micro needles in human cadaver skin and in different polymers which can serve as potential skin substitutes. The needles punctured the skin at a force of 52±22 mN after elastically deforming the skin for about 594±64 μm. The puncture force for a particular needle was consistent but varied substantially for different needles. The puncture force variation among the needles was attributed to the sharpness of the needle tip geometry. During these tests SEM observation of needles after skin penetration showed skin residues but only along a fraction of the needle length.

As a possible synthetic substitute for skin a range of materials with durometer ratings of 20A to 95A were screened. A 20A silicone displayed similar force vs. needle tip displacement behavior to that of the cadaver skin and was selected as the material of choice as a synthetic substitute for skin. A 50A silicone also exhibited similar behavior to that of skin but with 6 times greater resistance to penetrations than skin and therefore 50A silicone was considered as a good candidate for needle reliability testing. Reliability tests were carried out on a 250 needles from 3 different fabrication lots. In each case 50A was penetrated once to a full load of 1 kg with no needle fracture observed.

It was found that the needles deeply deformed the polymer but even after puncture did not penetrate through the materials to the full needle length. The actual length of the needle penetrated into the 20A silicone at full load of 50 g load cell was estimated by a nail polish technique and an aluminum sheet technique to be 60-80% of the full needle length. These observations are consistent with the observations of skin residue and lead to the conclusion that there is an air gap around the base of the needle.

1. INTRODUCTION

1.1 Motivation

Effectively transporting drugs into the body is a significant challenge. Oral delivery of drugs is the most common and convenient method, but is not always appropriate because drugs must survive the harsh environment of the gastrointestinal tract and first pass metabolism of the liver. More sensitive drugs, including proteins, are usually destroyed in the gastrointestinal tract and hence are administered by hypodermic injection, which requires medical expertise and also causes pain. In addition, bolus delivery from conventional injections reduces the effectiveness of drugs that would benefit from controlled release over time. As an alternative, transdermal patches provide convenient, time-release delivery that avoids the gastrointestinal tract. However, rates of delivery are often slow, because the skin's outer layer of stratum corneum severely limits diffusion of most compounds. Over the past few years, a variety of different microneedle designs have been fabricated to painlessly pierce the skin's stratum corneum and thereby transport drugs into the body.

1.2 General Background

In the recent past, Micro Electro Mechanical System (MEMS) technology has been applied to the design of novel drug delivery systems[1-6]. One such design uses silicon micro needles to achieve transdermal drug delivery in the form of micro-needles array patches[7,8]. These silicon needles provide several advantages over other drug delivery systems. They are painless during penetration into the skin, are non implantable and hence require no surgical procedure and have immunological consequences, can easily and conveniently be used requiring no trained personals such as nurses to

administer them, use a very large skin surface area to apply the patches, and finally offer an effective bypassing of the typical drug-degrading entero-hepatic portal circulation system.

Although several micro-needle designs have been proposed, not all are capable of inserting into the skin[9]. Successful drug delivery depends upon repeatable needle penetration under reasonable loads, without needle fracture. Hence understanding the relationship of the force required to insert the micro-needles into human skin, and the effect of needle tip geometry on this insertion force will allow improvements in design of the needle system.

Recently silicon micro-needles have been used to penetrate the epidermal barrier layer in a technology termed PyraDerm^{TM} by Apogee Technology[10]. These silicon micro needles need to be tested rigorously for reproducibility, but evaluation of microneedle array behavior depends on a fundamental understanding of the penetration behavior of individual needles. The goal of this research is therefore to carry out the following tests: finding the ability of a needle to penetrate the skin and the force needed to puncture the skin as well as estimating the contact area of the needle when penetrated into the skin to determine the dose of a drug, the variability of contact area of the needle as a function of applied force, and the variability of force needed to puncture as a function of number of needle for the design of an applicator in order to achieve a desired contact area for appropriate dose delivery.

However, carrying out these robust tests in human or animal skin is difficult and costly. Primarily the difficulty lies in collection and storage of tissues, and also textural variation due to age, species, and location of the skin. A synthetic substitute for skin is

highly homogeneous, insensitive to environmental conditions, and stable over long periods of time. It therefore serves as a more reliable material for the unambiguous, fundamental evaluation of needle behavior than natural skin. When chosen for greater resistance to penetration than skin, it also provides for a margin of safety with regard to needle reliability.

1.3 Thesis Contribution

This thesis describes:

1) A method of data acquisition of needle insertion and puncture forces.
2) Selection of synthetic skin substitute.
3) Determination of a scaling factor describing how the penetration force depends on the number of needles in the array.
4) A technique to estimate the contact area of the needle inside the material after puncture.

1.4 Organization

This thesis reports the results of experiments that study the force/penetration characteristics of the silicon micro needles into human cadaver skin and into different potential synthetic skin substitutes. This thesis is organized as follows. In section 2, the experimental system for measuring the force and the position of a micro-needle tip with respect to the surface of the skin is described. Section 3, describes the preparation of sample specimens for testing. Section 4 describes the various experiments that were carried out. The experimental results are presented and discussed in section 5 with conclusions and scope of future work in section 6.

2. EXPERIMENTAL EQUIPMENT

A schematic diagram of the measurement system is shown in the figure 2.1. The system consists of: the test frame, the driver for needle movement, the force sensor and its signal conditioning and the data acquisition and controls. The details of these system components are described here.

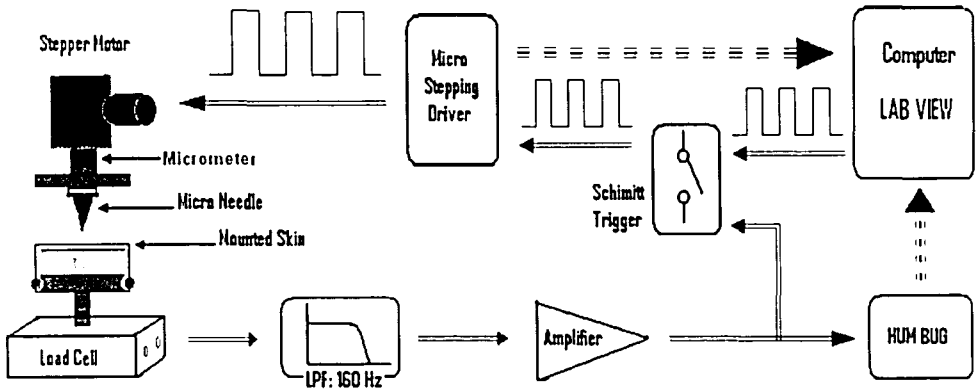

Figure 2.1 A schematic diagram of the measurement system. The stepper motor is driven by digital pulses generated in the LabVIEW. The force due to needle advance is sensed by a load cell. The load cell signal is conditioned before being fed into LabVIEW. The Needle tip position and the force data are continuously acquired in LabVIEW and shown in red dotted arrows.

In operation, a stepper motor coupled to a micrometer drives a micro-needle at a constant rate downward against a mounted human cadaver skin sample. The stepper motor is driven by custom LabVIEW software and dedicated motor control hardware. The force applied to the sample by the micro-needle is measured with a conventional load cell, and fed to LabVIEW for storage and analysis. An electronic circuit shuts off the needle advance at a desired load level to prevent damage to the load cell. Needle extension and retraction are under LabVIEW control.

2.1 Test Frame

The test frame consists of two 25 mm diameter thick-wall aluminum tubes filled with vibration damping material. The base of the tubes is mounted on an anti-vibration

table. The stepper motor, enclosed in an aluminum shielding box, is mounted via anti-vibration supports to a plate that is bolted to the two vertical tubes. A 50 mm micrometer is mounted to another plate between the vertical tubes. The micrometer is connected to the stepper motor through a custom sliding drive and neo flex coupling in such a way that the angular rotation of the stepper motor is translated into vertical displacement of the micrometer at a selectable rate. The load cell is mounted to a manually driven X-Y micrometer stage which allows translation of the load cell (and the skin sample mounted to it) so that multiple tests may be performed at different positions on a single skin sample.

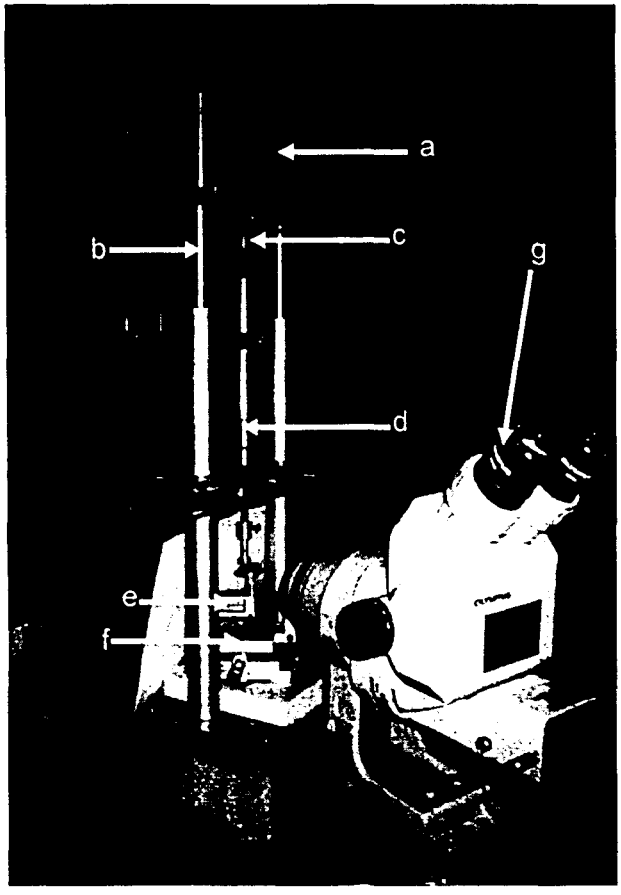

Figure 2.2 The test frame. a)Stepper motor enclosed in aluminum box b)Aluminum tube filled with vibration damping material c)Neo flex coupling and slider d)Micrometer e)Load cell f)X-Y Stage g) Stereo microscope.

table. The stepper motor, enclosed in an aluminum shielding box, is mounted via anti-vibration supports to a plate that is bolted to the two vertical tubes. A 50 mm micrometer is mounted to another plate between the vertical tubes. The micrometer is connected to the stepper motor through a custom sliding drive and neo flex coupling in such a way that the angular rotation of the stepper motor is translated into vertical displacement of the micrometer at a selectable rate. The load cell is mounted to a manually driven X-Y micrometer stage which allows translation of the load cell and the skin sample mounted to it so that multiple tests may be performed at different positions on a single skin sample.

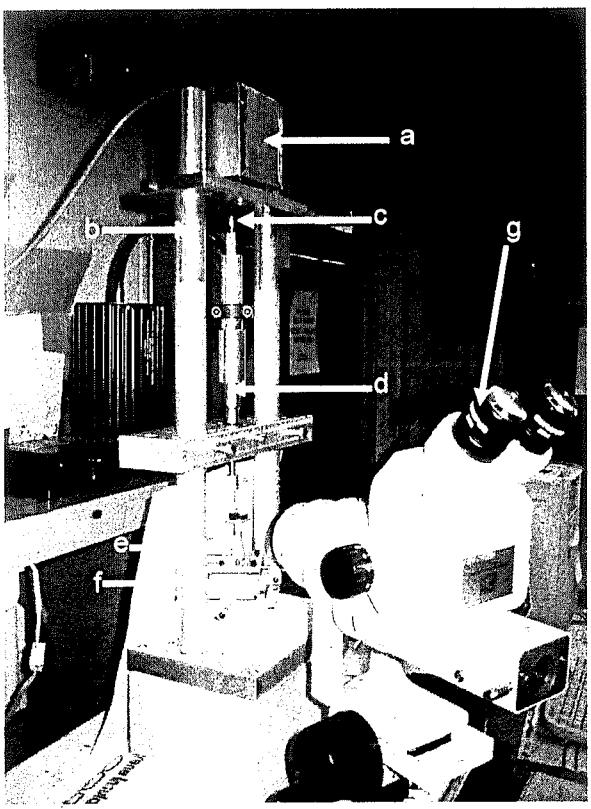

Figure 2.2 The test frame. a)Stepper motor enclosed in aluminum box b)Aluminum tube filled with vibration damping material c)Neo flex coupling and slider d)Micrometer e)Load cell f)X-Y Stage g) Stereo microscope

2.2 Needle Movement

The needle displacement is achieved by the micrometer movement, driven by the bipolar stepper motor STP-MTR-23079 from Automation Direct. The stepping system power supply STP-PWR-3204 is used to power the stepper motor. The stepper motor makes 200 steps for one complete revolution with a basic stepping angle of 1.8°. A micro stepping drive STP-DRV-4035 provides selectable micro stepping so that there are 400, 1000, 2000 or 10,000 steps per revolution. The rate at which pulses are supplied to the micro-stepper and the choice of the micro-stepping multiplier allows wide adjustment of micrometer speed. In the experiments to be described below a speed of 1 mm/sec has been used both on advance and retraction of the micro-needle.

2.3 Force Sensor and Signal Conditioning

A GSO series precision 50 gram load cell sensor from Transducer Techniques is mounted rigidly on the XY stage with a piece of silicone polymer sandwiched in between. The load cell, which has excellent compliance and temperature stability, is used in the compression mode. The rated output for the sensor is 1millivolt per volt nominal. DC excitation is at 10 volts. The output of the load cell is fed to a Transducer Techniques TMO-2 module. It is a complete bipolar differential bridge amplifier/signal conditioner. The TMO-2 unit supplies constant transducer bridge excitation voltage, as well as balance and span adjustment via precision 10 turn pots. Full scale output is specified as plus or minus 10 VDC. The standard low pass filter default band width of 16Hz was increased to160 Hz by internal capacitor changes so as to provide more faithful dynamic loading response.

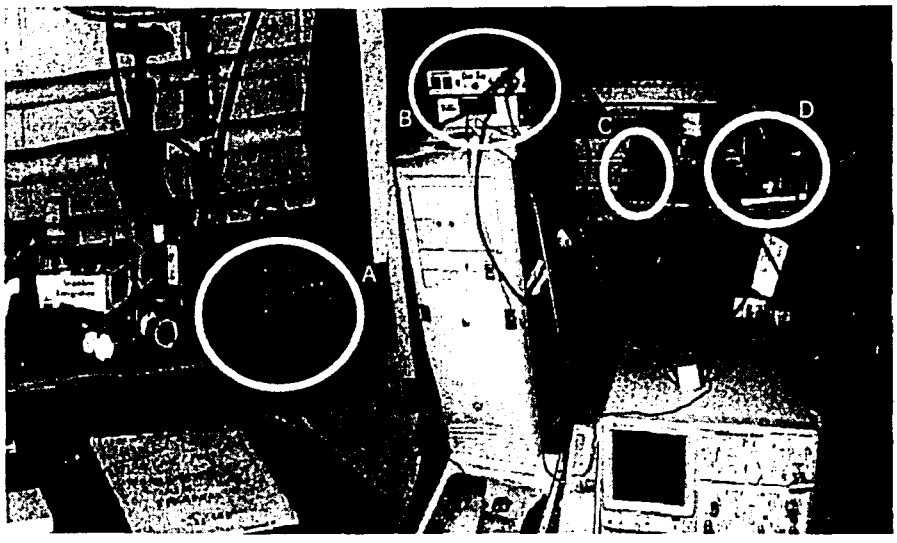

Figure 2.3 The force sensor signal conditioning units. A).TMO-2 Amplifier B). Humbug and LabVIEW interface C). Micro stepping driver D). Schimitt trigger safety switch.

The output of signal conditioner TMO-2 is supplied in parallel to a HumBug line frequency noise eliminator and to a Schimitt trigger safety switch module. The HumBug effectively eliminates the 60Hz power line interference from the measurement signal. The Schmidtt trigger shuts off pulses to the microstepping controller at a preselected load to prevent overloading of load cell.

2.4 Data Acquisition and Control

An integrated, high performance LabVIEW 8 virtual instrumentation data acquisition system controls the micro-stepper pulse rate, counts pulses supplied to the stepper to keep track of micro-needle position, and measures the output of the load cell as shown in figure 2.4. Data can be acquired at a rate of 1000 samples per second. Data acquisition is achieved using a National Instruments high speed, 16 bit resolution, multifunction M series PCI 6251 DAQ card and Daqmx driver software.

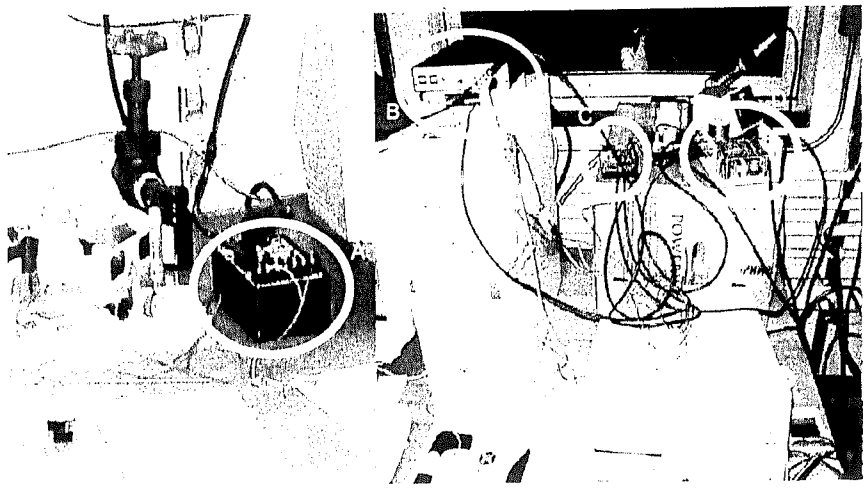

Figure 2.3 The force sensor signal conditioning units. A) LMO-2 Amplifier B) Humbug and LabVIEW interface C) Micro-stepping driver D) Schmitt trigger safety switch

The output of signal conditioner LMO-2 is supplied in parallel to a HumBug line frequency noise eliminator and to a Schimitt trigger safety switch module. The HumBug effectively eliminates the 60Hz power line interference from the measurement signal. The Schmidt trigger shuts off pulses to the microstepping controller at a preselected load to prevent overloading of load cell.

2.4 Data Acquisition and Control

An integrated, high performance LabVIEW 8 virtual instrumentation data acquisition system controls the micro-stepper pulse rate, counts pulses supplied to the stepper to keep track of micro-needle position, and measures the output of the load cell as shown in figure 2.4. Data can be acquired at a rate of 1000 samples per second. Data acquisition is achieved using a National Instruments high speed, 16 bit resolution, multifunction M series PCI 6251 DAQ card and Daqmx driver software.

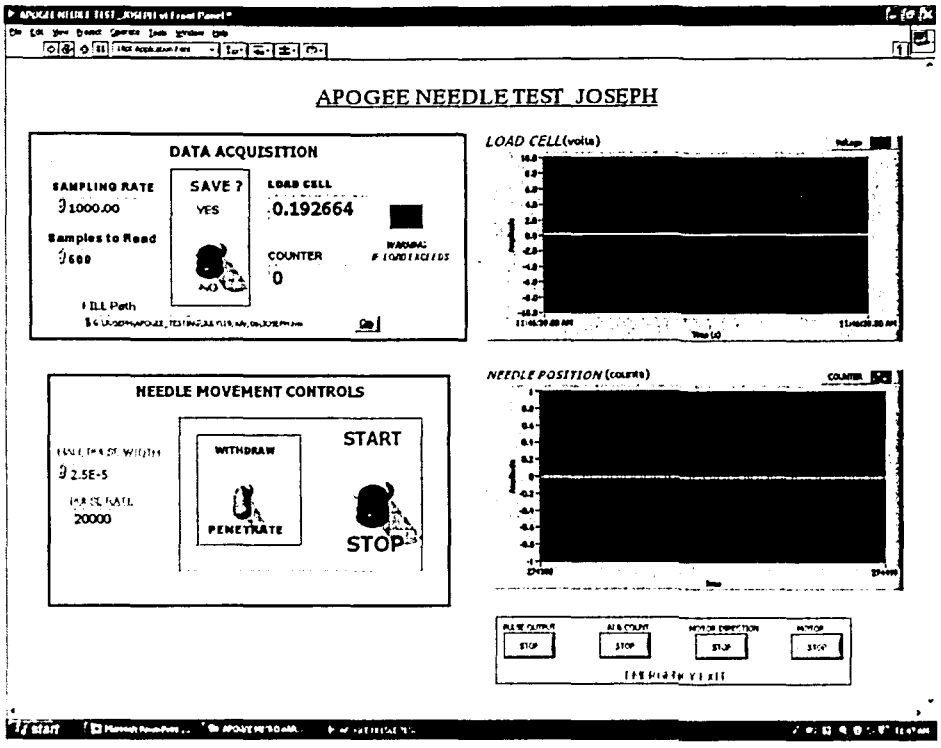

Figure 2.4 The front panel of the LabVIEW virtual instrument. The controls for data acquisition are penetration rate, needle direction, sampling rate, and samples to read. The values of load cell and the needle tip position during acquisition are displayed in charts.

2.5 Test Setup Validation

The 50 g and 1 kg load cells were both calibrated with NIST-traceable static weights prior to testing. In addition, needle penetrations into each of the polymers were performed with both load cells, using the same needle for each test at 1 mm/s. As seen in figure 2.5, the overlap between the loading results for the two load cells is excellent, proving that data gathered with one cell can be safely compared with data gathered with the other cell. This makes it possible to test single needles with high resolution using the 50 g load cell, and single needles and arrays at high load using the 1 kg load cell. The measurement noise limit was found to be 3 mN.

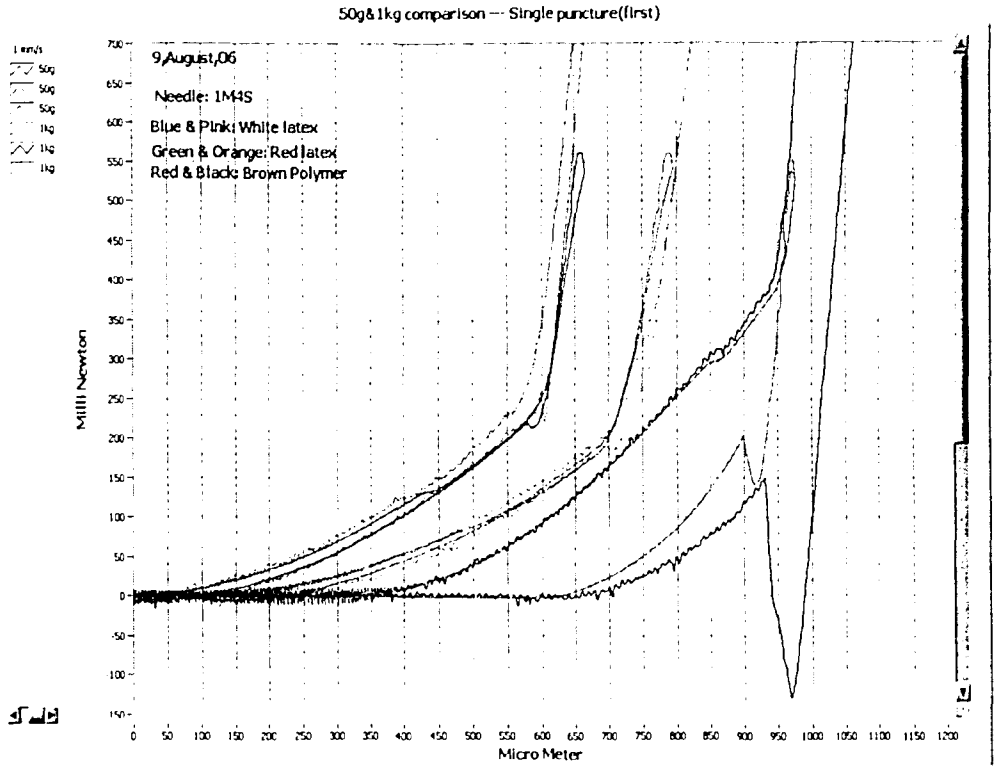

Figure 2.5 Comparisons of 50g and 1kg load cell response for three polymers. The white latex, red latex, and brown polymer (silicone), have Shore A hardness values of 35, 40, and 50 respectively. Excellent agreement between the load cells is evident. Differences in behavior for the brown polymer on retraction are attributed to greater adhesion between the needle die and the polymer associated with higher load.

3. MATERIALS AND METHODS

3.1 Micro-Needle

There are many types of materials, shapes and methods of processing that can be used to fabricate micro-needles[11]. The silicon needles used in this study were fabricated by anisotropic chemical etching. They are eight-sided cones with a half cone angle of approximately 20° and a length of 600 um, centered on a 2 mm x 2 mm square silicon die. These needles were supplied by Apogee Technology, Inc. An optical image of a micro-needle mounted on a stub is shown in figure 3.1a. figure 3.1d is a SEM end view of a micro-needle. It shows the non regular octagon.

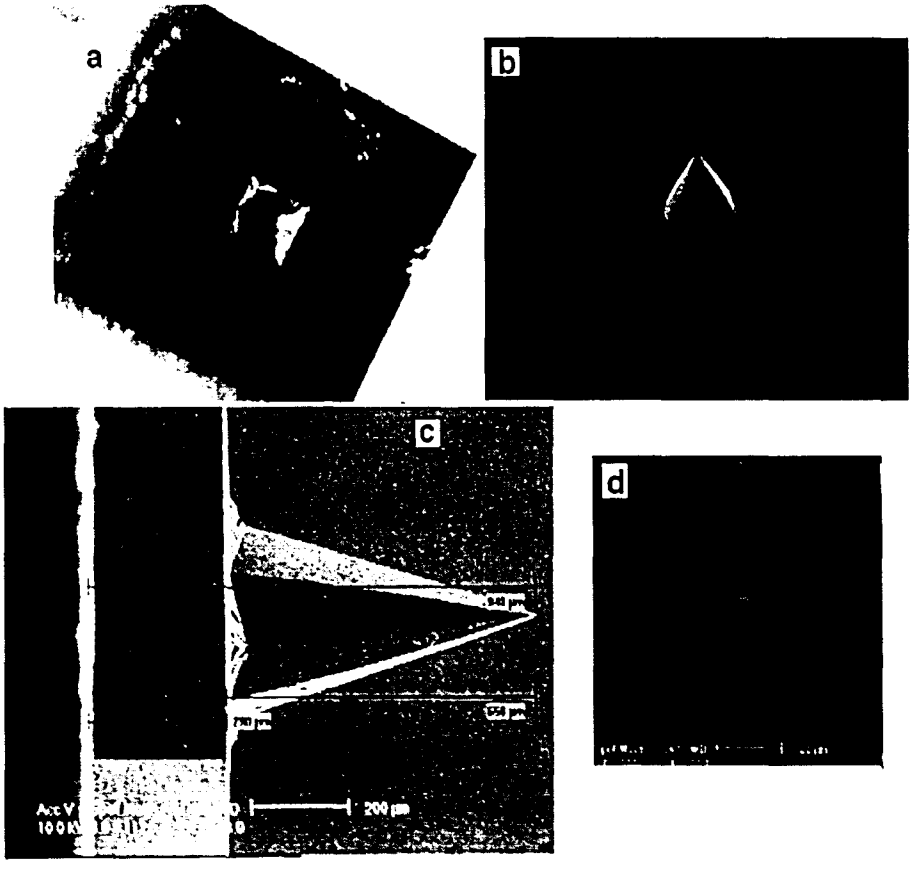

Figure 3.1 Pictures of a mounted micro needle a) optical image of micro needle in a 2 mm x 2 mm die base b) SEM image at 45deg tilt c)SEM image at 90 deg tilt shows the die and needle height d) head on view of SEM image of micro needle shows octagonal cone.

3. MATERIALS AND METHODS

3.1 Micro-Needle

There are many types of materials, shapes and methods of processing that can be used to fabricate micro-needles[11]. The silicon needles used in this study were fabricated by anisotropic chemical etching. They are eight-sided cones with a half cone angle of approximately 20° and a length of 600 um, centered on a 2 mm x 2 mm square silicon die. These needles were supplied by Apogee Technology, Inc. An optical image of a micro-needle mounted on a stub is shown in figure 3.1a. figure 3.1d is a SEM end view of a micro-needle. It shows the non regular octagon.

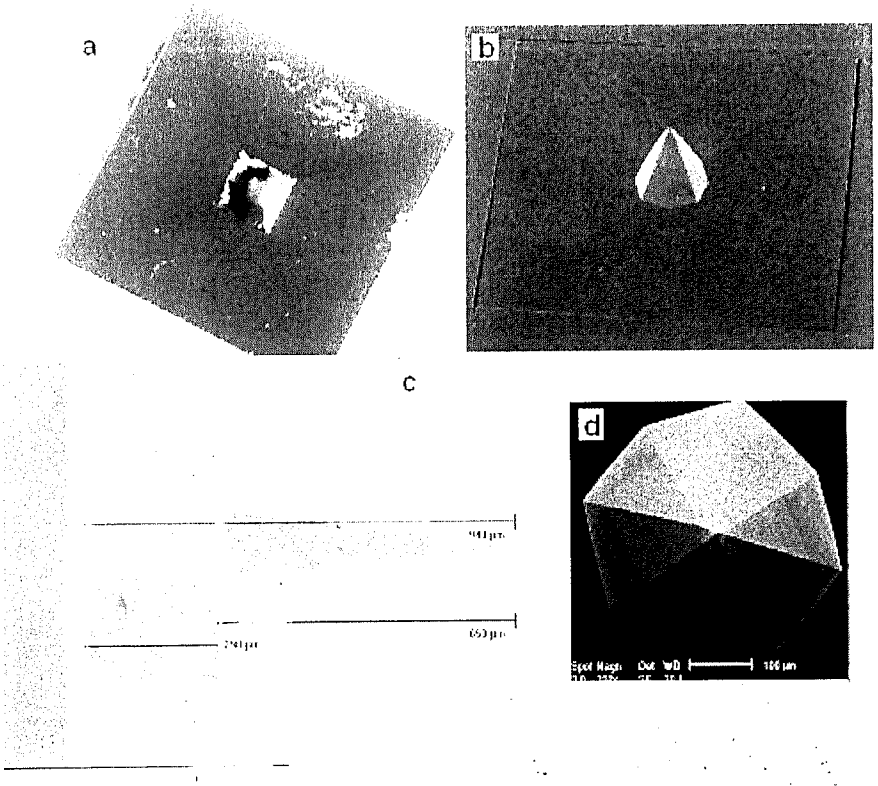

Figure 3.1 Pictures of a mounted micro needle a) optical image of micro needle in a 2 mm x 2 mm die base b) SEM image at 45deg tilt c)SEM image at 90 deg tilt shows the die and needle height d) head on view of SEM image of micro needle shows octagonal cone.

3.2 Polymers

Several materials were selected for initial normal-angle penetration evaluation on the basis of their durometer hardness characteristics. Medical literature shows that durometer measurement, a standard polymer hardness test, can be used to characterize human skin with regard to resistance to blunt indentation. Soft materials are often measured on the Shore OO or O scales, while harder materials are measured on the Shore A or D scales.

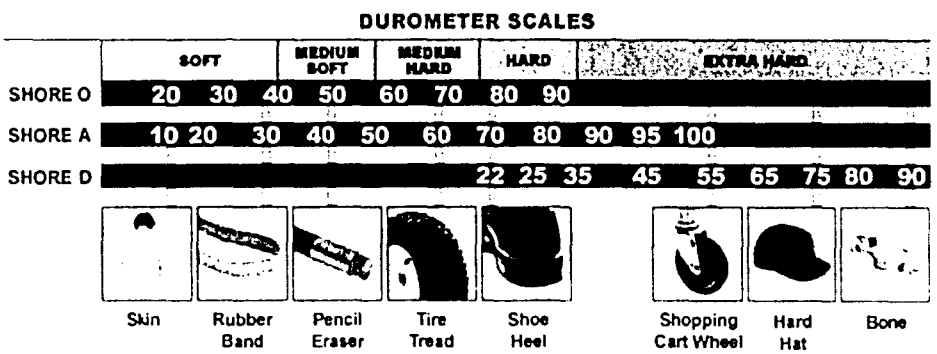

Figure 3.2 Approximate correlations between durometer scales and common materials [modified from a figure found at www.mcmaster.com].

On the durometer Shore O scale, normal skin has been measured as approximately 25±5[12]. Skin experiencing induration due to lipodermatosclerosis was measured at approximately Shore O 45-65. Likewise, the durometer has been shown to be useful for characterization of hypertrophic scarring. A recent study reported Shore O durometer measurements in the range of 30 to 70 for hypertrophic scar tissue associated with burns[13]. The range of 25 to 70 on the Shore O scale corresponds approximately to Shore A 15 to 60. The Shore D scale is for very hard polymers, and has little overlap with the relevant portion of the Shore O scale. A depiction of the durometer scales is shown in figure 3.2. Based on the cited medical literature, we sought materials with durometer values equal or greater than skin. Accordingly, we selected a range of

materials with durometer ratings of 20A to 95A. These include natural latex, silicones, several different formulations of polyurethane, and Formica.

3.3 Micro Needle Mounting Procedure

Micro needles and needle arrays were mounted onto standard SEM specimen stubs, modified slightly to create threaded shafts. The specimen stubs were carefully polished with an engineer's file to ensure a flat surface. The two components of an electrically conducting, silver-filled, medium viscosity epoxy (TRA-DUCT 2907) were thoroughly mixed, in the BIPAX mixing-dispenser provided with the product, by removing the clamp. The components were mixed well until color was uniform throughout. Then a thin layer of the completely mixed epoxy was applied onto the stubs for needle die mounting. An individual needle die from the chosen wafer and wafer location was plucked out and mounted onto the center of the epoxy coated stub, as shown in Figure 3.3, with the help of plastic tweezers. Then the needle die was slowly dragged to construct different kinds of arrays such as 1x2, 1x3, 1x4, 2x2, 2x3, 2x4, and 3x3. A 3 x 3 matrix of tightly-packed needle dies is shown in figure 3.4. The needle die/stub assembly was left overnight for curing. On the next day the specimen stubs were kept at 50 C for 2 hours for reliable epoxy curing.

The standard identification scheme for labeling all tested needles incorporates Apogee's lot and wafer numbering system. For example, a sample labeled A6-1-3RS has as its first four letters the Apogee number for that particular wafer and lot. R indicates the location on the wafer from which the needle or array was extracted (the possible locations are Right, Top, Left, Bottom and Center). S stands for single needle; an array would be

labeled A. If an SEM image is taken post-test, the sample name will have T as the last letter (images of untested type will have no corresponding additional letter).

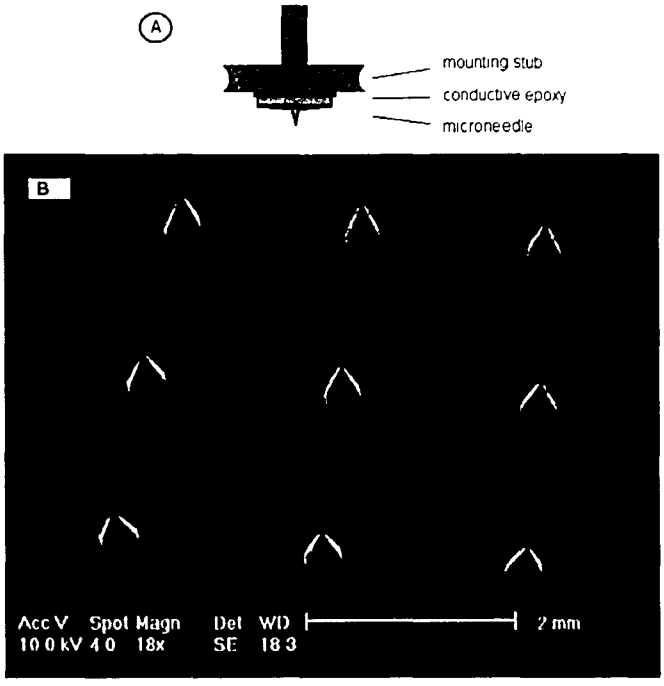

Figure 3.3 A. Schematic diagram illustrating the mounting configuration for a needle die B. SEM image of 3x3 arrays constructed.

3.4 Skin Specimen Preparation Procedure

A sheet of cadaver skin, stored at minus 80 degrees in a freezer at Rutgers University was transferred to a dry ice cooler and brought to Lehigh University on the day of testing. After thawing for one hour at room temperature, many one inch square pieces were cut from a portion of the skin using surgical scissors. All the skin pieces were hydrated for more than 30 minutes at 37 C in phosphate buffered saline solution. Each sample was then stretched over a load cell stub to which a disc of white latex (Shore hardness 35A) had already been glued using cyanoacrylate glue, as shown in Figure 3.4. The latex is 1/8 inch thick. Stretching was accomplished using an O-ring that acts like an embroidery hoop, clamping the skin specimen over the side of the circular stub. A

customized tool was used to apply the O-ring which ensures uniform distribution of tension and also mechanically holds the skin. Any excess skin hanging down the side of the stub was trimmed out using surgical scissors.

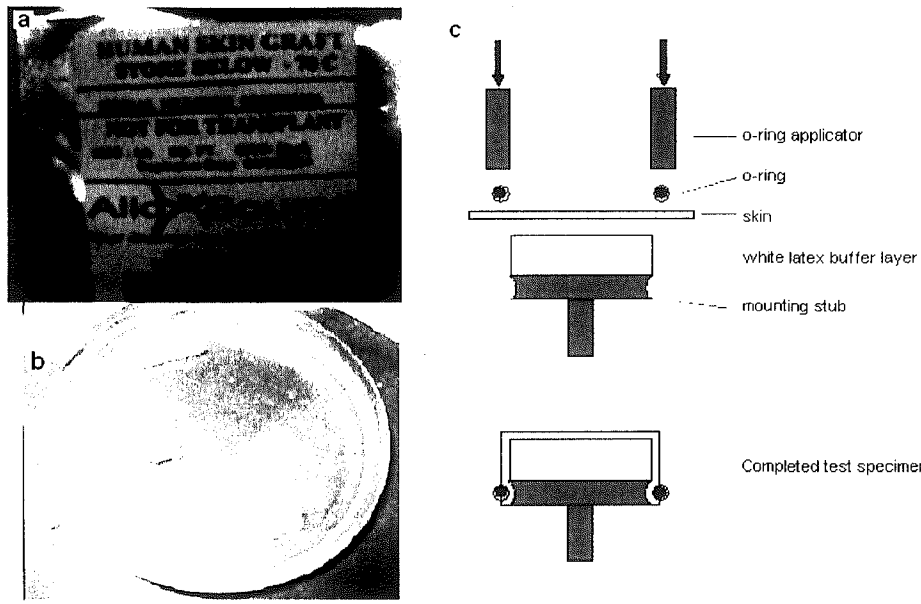

Figure 3.4 a) Human cadaver skin graft stored at minus 80 deg. b) Thawed and hydrated skin in Petri dish. c) Schematic diagram of assembly of a human cadaver skin penetration specimen (not to scale).

3.5 Synthetic Polymer Specimen Preparation Procedure

Discs of the 1/8 inch thick polymer sheets with adhesive coating on one side were cut and mounted on metal specimen stubs. The non-adhesive polymers were glued to the stub using cyanoacrylate. Each polymer disc was gently pressed on to the stub and left for 5 minutes to cure.

4. EXPERIMENTS

4.1 Human Cadaver Skin Testing

The skin specimens were prepared according to the procedure discussed in section 3.4 using threaded load cell stubs as shown in figure 4.1a. The threaded end of the stub was screwed into the load cell for testing as shown in figure 4.1b. Systematic tests with single needles and arrays were carried out, as discussed below using both load cells (50 g and 1 kg). The single needle or array was advanced by the motor drive at a constant rate of 1.0 mm/sec. Computer data acquisition of load and needle displacement were initiated with a sampling rate of 1000 samples per second and stored continuously. Once the load cell maximum capacity was reached due to the penetration of the needles into the skin specimen, the needle motion was stopped automatically by the Schmidt trigger safety switch. After holding the needle at that maximum load limit for one or two seconds, the needle was retracted at the same rate. During the needle withdrawal, once the needle was clearly out of contact with the skin the direction of needle movement was reversed to penetrate again at the same position on the skin. A full test consisted of four penetration cycles in a single location using a single needle or array of needles. After the four penetration and withdrawal cycles were completed the data acquisition was stopped. The skin sample was translated approximately 1 mm to position a new location on the skin under the needle for further testing. Each micro needle or array was used in four different locations on a single skin sample to check the repeatability. Additional tests with the same skin, but with different needles, were performed to examine the variability among the needles.

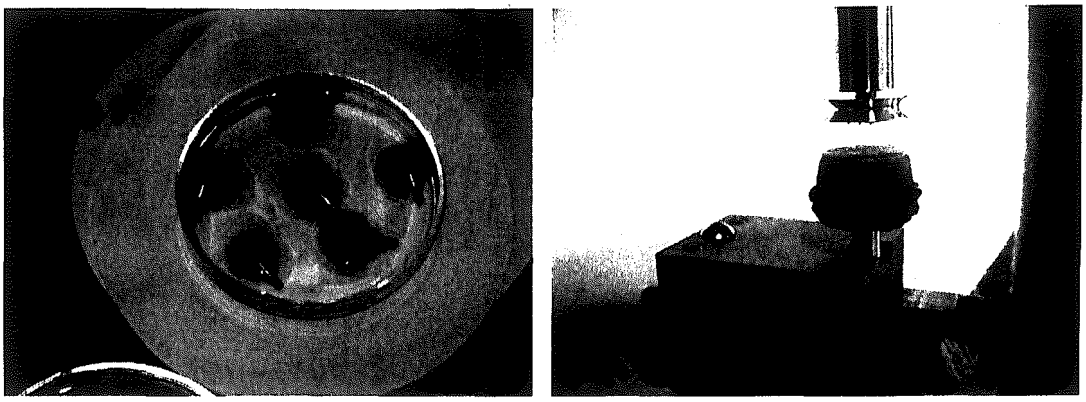

Figure 4.1 Skin mounted according to section 3.4 (a) Skin samples in phosphate buffered saline solution. (b) One sample mounted in the test system. A needle array is suspended above the skin sample, and the load cell is visible supporting the specimen.

4.2 Synthetic Polymer Materials Testing

Materials with durometer ratings of 20A to 95A were selected based on medical literature. These include natural latex, silicones, several different formulations of polyurethane, and Formica. The selected synthetic materials specimens were prepared according to the procedure discussed in the section 3.5 using threaded load cell stubs. The threaded end of the stub was screwed into the load cell for testing.

4.2.1 Synthetic Skin Model Screening Tests

Systematic tests with single needles similar to skin tests were carried out using the 50 g load cell for the purpose of selecting an appropriate synthetic skin model. The single needle was advanced by the motor drive at a constant rate of 1.0 mm/sec. Computer data acquisition of load and needle displacement were initiated with a sampling rate of 1000 samples per second and stored continuously. Once the load cell maximum capacity was reached due to the penetration of the needle into the synthetic material specimen, the needle motion was stopped automatically by the Schmidt trigger safety switch. After holding the needle at that maximum load limit for one or two seconds, the needle was retracted at the same rate. During the needle withdrawal, as soon as the needle was

clearly out of contact with the synthetic material the direction of needle movement was reversed to penetrate again at the same position on the material. A full test consisted of four penetration cycles in a single location using a single needle. After the four penetration and withdrawal cycles were completed the data acquisition was stopped. The synthetic material sample was translated approximately 1 mm to position a new location on the material under the needle for further testing. Each micro needle was used in four different locations on a single synthetic material sample to check the repeatability.

4.2.2 Needle Reliability Tests

Systematic tests of mounted single needles and arrays were carried out in 50A silicone using the 1 kg load cell. The selection of the 50A silicone for needle reliability tests is discussed in Chapter 5. The single needle or array was advanced by the motor drive at a constant rate of 1.0 mm/sec. Computer data acquisition of load and needle displacement were initiated with a sampling rate of 1000 samples per second and stored continuously. Once the load cell maximum capacity was reached due to the penetration of the needle into the 50A silicone specimen, the needle motion was stopped automatically by the Schmidt trigger safety switch. After holding the needle at that maximum load limit for one or two seconds, the needle was retracted to the initial starting position at the same rate. The data acquisition was stopped and the tested needles were removed from the test frame for SEM imaging.

4.3 Video Indentation

The penetration of a single needle into a transparent polymer was captured in video. The single needle was advanced at a constant rate of 0.01mm/sec into 1.5 mm thickness transparent silicone to a predetermined distance from the surface of the

material. The predetermined distance was chosen in such a way that the load cell was not overloaded beyond its rated value of 2500 mN. The force and displacement data was acquired at 100 samples per second while the movement of the needle into the transparent material was captured through the polymer using an inverted microscope coupled with a video camera coder. The video was then edited into many picture slides and correlated with the load/displacement data.

4.4 Nail Polish Technique

The mounted single needles were tested systematically at the rate of 1.0 mm/sec using the 50 g load cell in 20A silicone polymer to determine the punctured contact area of the material with the needle. The selection of the 20A silicone material for this test will be discussed in the next chapter. The needle was brought down at a slow rate of 0.1mm/s close to the surface of the 20A silicone material which was mounted on the load cell. The needle was further advanced towards the mounted 20A polymer at 0.01 mm/s until a rise in load was observed. The point at which there is a rise in load was considered to be the initial contact point of the needle with the polymer. At this initial contact point the further needle advancement was stopped. Then the needle was retracted to a fixed distance of 3 mm from the initial contact point. This ensured enough working space between the needle tip and the surface of polymer without any hindrance. Then a thin layer of Nail Polish was applied using the nail polish brush. Immediately, the needle was advanced to a predetermined distance at 1.0 mm/s. The predetermined distance consisted of the distance needed to reach the initial contact point plus an additional distance to advance the needle further into the 20A polymer from its surface. Once the needle reached the predetermined distance, it was retracted back to the previous position after a

stationery period of 3-4 seconds. Then both the needle stub and polymer mounted load cell stub were dismantled from the measurement system for imaging and analysis. The tested needle was photographed using the stereomicroscope, coupled with a digital camera at a total optical magnification of 44 times. After stereo imaging the needle was rinsed in an acetone solution to remove the nail polish coating. The needle was visually examined to check for any damage before mounting for another test. The needle was then tested into new piece of polymer as before. Several tests were done at different predetermined distances: 200, 300, 400, 500 and 600 microns into the material from the point of initial surface contact.

4.5 Aluminum Foil Technique

An aluminum foil sheet of thickness 25 microns was placed on the mounted 20A silicon specimen before advancing the needle. The needle was advanced at 1mm/sec to a predetermined distance from the surface of the material. Once the needle tip reached the predetermined distance, it was retraced back to its original position at the same rate and the tested material was stored for analysis.

5. RESULTS AND DISCUSSION

5.1 Single Needle Penetration into Skin

The position of the micro needle tip and the force acting on the micro needle versus time during a cycle as (described in section 4.1) are shown in figure 5.1. After starting data recording at time zero, the micrometer movement is started after an additional time interval A. There is no change in load for a period of time before the micro needle has reached the surface of the skin specimen (section B). Once the micro needle tip touches the surface of the skin the force starts to increase (section C). After reaching the load cell limit, the safety switch shuts off the pulses sent to the motor and hence there is no increase in the pulses counted. During this holding period, the load decreases without needle motion due to relaxation of the stress of insertion (section D1). After a relaxation of 80 mN, the safety switch engages again and the micro needle again advances to the load cell limit at which point the pulses are shut off (section D2). The final decrease in counter value and the rapid fall in load are due to withdrawal of the micro needle (section E).

Figure 5.2 shows micro needle force verses the micro needle tip position, replotting the data of Figure 5.1. The load cell has a finite compliance (it was determined to be 0.142 μm/mN) so that part of the total micro needle tip advance is actually displacement of the load cell. Figure 5.2 has been corrected for load cell compliance so that the needle displacement values shown are a measure of the needle tip motion with respect to the undeformed surface of the skin. The load cell reading before needle tip contact (due to the weight of the skin sample assembly) has been subtracted so that the loads shown are only loads associated with micro needle contact with the skin.

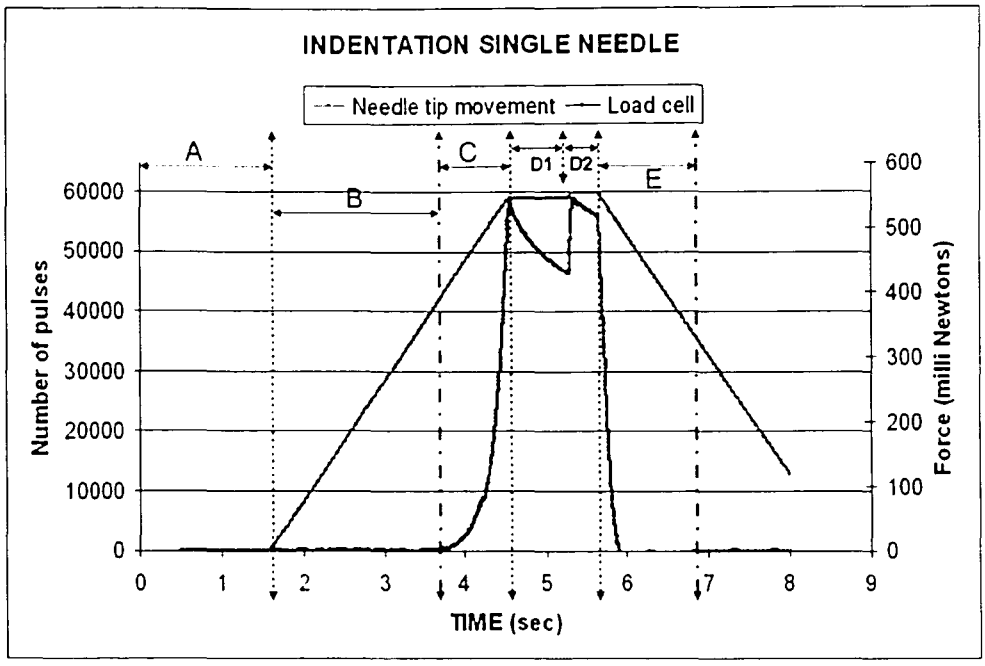

Figure 5.1 The position of needle tip and force acting on the micro needle when penetrated into human cadaver skin. The different time periods of penetration in the withdrawal cycle are also segmented.

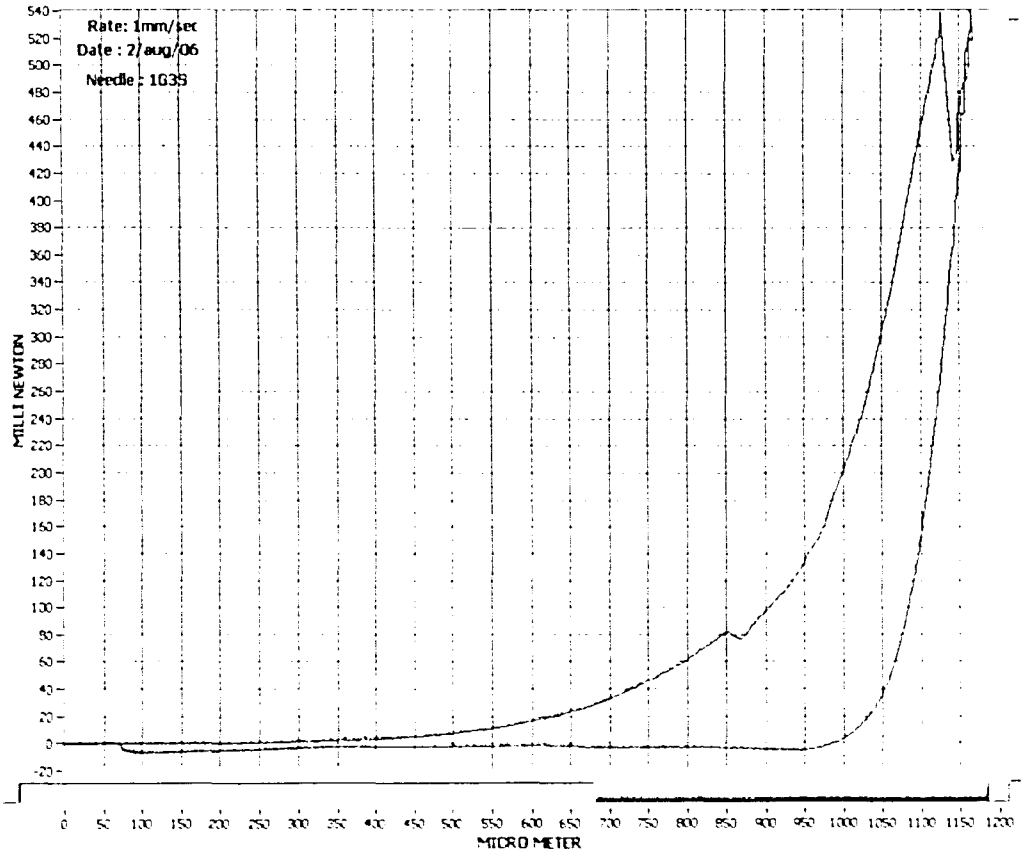

Figure 5.2 The force vs. micro needle tip advancement from the surface of the skin. The sudden small drop in the load due puncture event is evident at 80 mN.

In the smoothly rising loading curve, one unique event is evident: a sudden small drop in load at a load value of approximately 80 mN. We interpret this drop as puncture of the skin by the tip of the micro needle. At lower loads, before this event, the load increases smoothly as the needle begins to deform the skin. After the puncture event the load again rises as the needle continues to move into the skin, cutting and further deforming the skin around the hole, and the silicon die comes into contact with the skin. A downward jog in load is expected at puncture as part of the elastic strain energy of skin deformation is suddenly released. Figure 5.3 shows the same data as in figure 5.2 but on a finer load scale. The position of the micro needle tip at the touch point on the skin is identified as 200 μm. From this touch point it is interesting to note that the puncture event occurs after the needle has moved into the skin (deforming it) a distance of approximately 650 microns, comparable to the length of the micro needle.

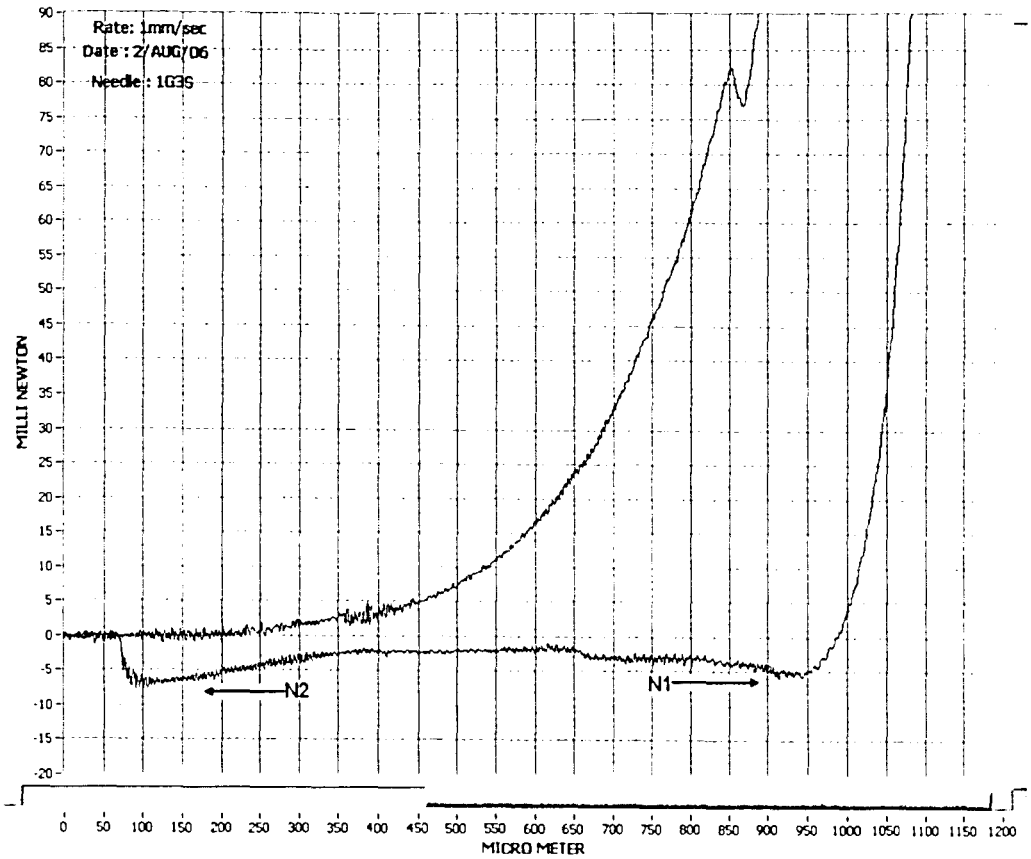

Figure 5.3 shows the force vs. micro needle tip advancement from the surface of the skin. The magnified curve shows two negative load drops during needle withdrawal. The first drop, marked N1, is due to die/skin adhesion, while the drop at N2 is due to surface tension of surface fluid.

In the unloading curve, the force decreases rapidly as the micro needle is withdrawn and has dropped to zero by about 200 μm after withdrawal begins. The steep fall in force is attributed to the reduction of skin compression by the large area (4 mm^2) of micro needle die contact with the skin as the micro needle is pulled from the puncture hole. A further drop in the force value to −6 mN at 950 microns, as seen in figure 5.3 marked as N1, we attribute to adhesion of the skin with the micro needle die. Another negative load drop of 8 mN at 100 microns (marked as N2) is also evident when the needle tip is withdrawn further than its initial touch point at 200 microns. During experiments it was observed that a drop of fluid oozed out from the skin at the puncture

spot and we suggest that the negative load drop at 100 microns is due to surface tension of the fluid with the needle tip which is now completely withdrawn from the skin.

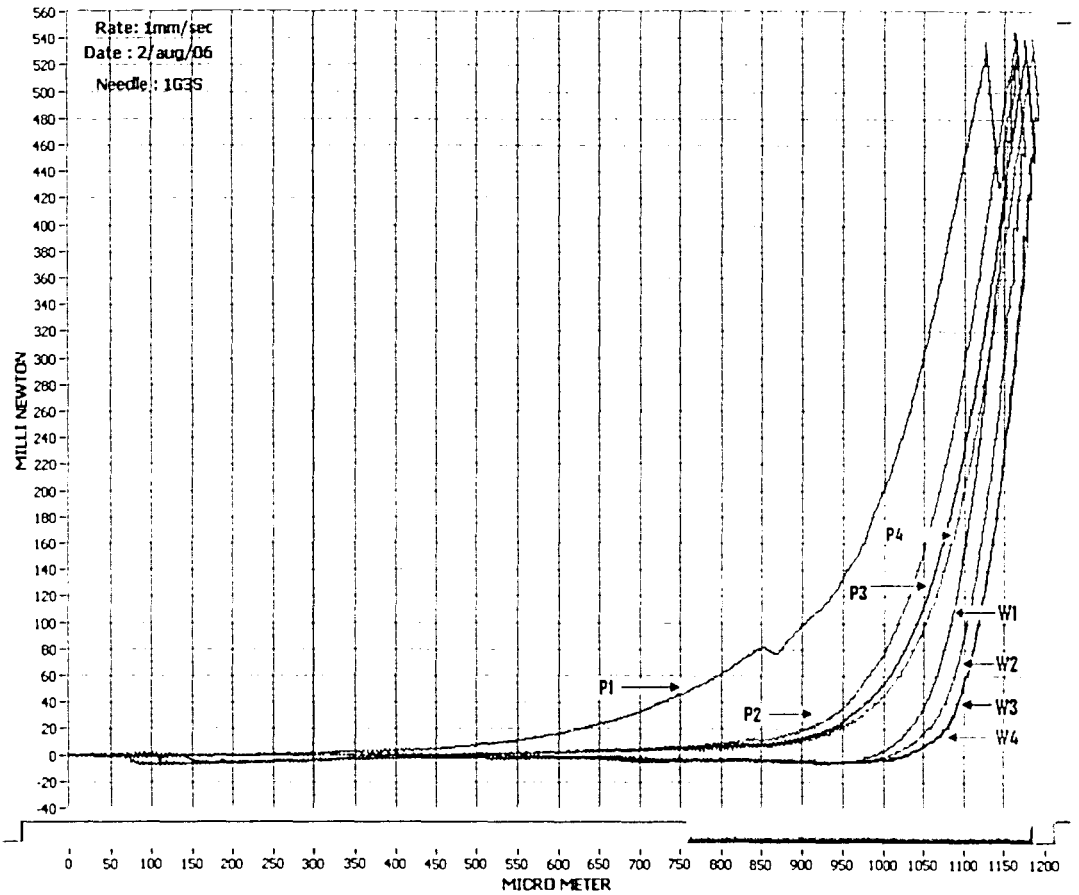

Figure 5.4 The force vs. needle tip movement of a single needle penetrating human cadaver skin. The test consists of four penetrations (labelled P1, P2, P3 & P4) and withdrawals (labelled W1, W2, W3 & W4) at one particular location on the skin. A puncture event is visible as a load drop only in the first penetration curve.

Figure 5.4 shows the force vs. displacement of the micro needle tip during multiple penetrations at a single location on the skin. When the four successive penetrations are compared during loading, the elastic deformation of the skin before puncture and the puncture load drop, are observed in the first penetration only. Such features are not evident in the 2^{nd}, 3^{rd} and 4^{th} penetrations. This is expected since the needle tip actually travels into the hole created during the first penetration. The steep rise in force after 900 microns during subsequent loadings is primarily due to the compression

of the skin by the needle die. The shape of the rise provides a measure of the effective compressive modulus of the skin. These compressions of the skin over the die area do not come back to the original position of the skin during the very short time in which these four penetrations have been made. This causes the steep load rise during the 2nd, 3rd and 4th insertion to be displaced to a slightly larger distance with each iteration. The shapes of the unloading curves in all the four penetration cycles are the same showing only shifts due to skin compression over the die area.

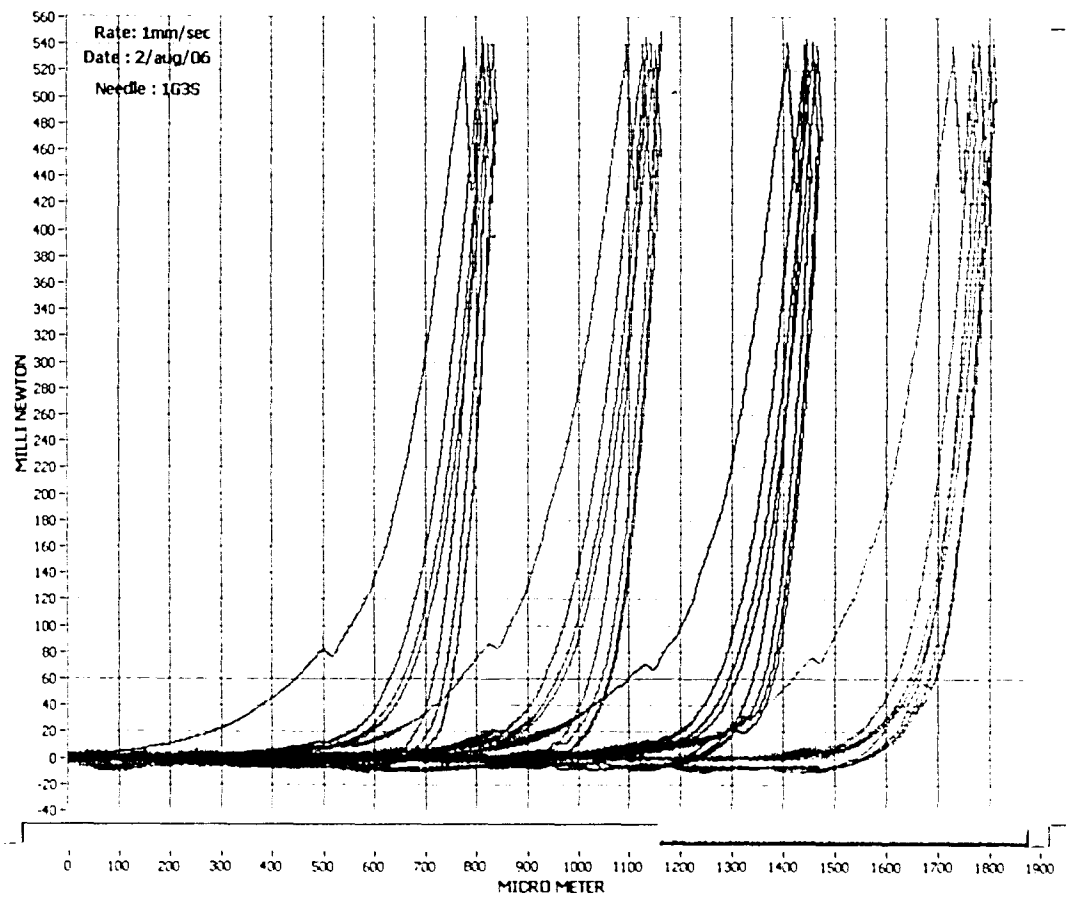

Figure 5.5 The tests of a particular micro needle at four different locations of skin. Each test consists of four insertions at one location, after which the skin sample is moved to a new location (a different color, offset for clarity). A puncture event is visible as a load drop only in the first penetration curve of each test location.

The cycles of penetration and withdrawal at four different locations on the skin for a particular micro needle tip are displayed in the figure 5.5. The force required to puncture

a skin sample at four different locations for a given micro needle tip is very similar (at least for needles ID3S & 1G3S). However, the variation in the puncture force for different needles is substantial as shown in table 5.1, for the three needles that were tested.

SPOT	Needle:1D3S		Needle:1G3S		Needle:1F3S	
	Puncture Force (mN)	Needle tip Travel distance (μm)	Puncture Force (mN)	Needle tip Travel distance (μm)	Puncture Force (mN)	Needle tip Travel distance (μm)
Location one	48	690	82	650	41	570
Location two	52	625	87	650	30	485
Location Three	49	580	71	620	23	520
Location Four	46	650	76	580	20	510
Averages	48.8±2.5	636±46	79±7	625± 33	28.5±9	521± 35

Table 5.1 shows the force and micro needle displacement of the needles when penetrated into the human cadaver skin.

An SEM image of the tested micro needle is shown in figure 5.6. Before testing in skin the micro needle is smooth and shiny (figure 3.1). After testing, the sticking of skin debris on the smooth slanting surfaces of the micro needle is very distinct. Note that the skin debris is present only at a fraction of the total needle height from its tip, which is believed to be the actual portion of the total needle length that penetrated into the skin. Moreover, two distinct micro needle indentation features are noticed in the optical image of the tested skin sample, shown in figure 5.7. First, the presence of a small hole confirming that puncture occurred. Second, a larger concave circular deformation of the skin around the punctured hole, implying that certain portion of the micro needle tip is not in contact with the skin even at full loading. There is skin deformation around the

micro needle: the indentation of the skin is not just the shape of the micro needle. This suggests the possible presence of an air gap between the needle and the skin around the base of the needle at full loading as sketched in the figure 5.8. This supposition is further supported by the presence of debris on the die surface beginning a certain distance from the needle base.

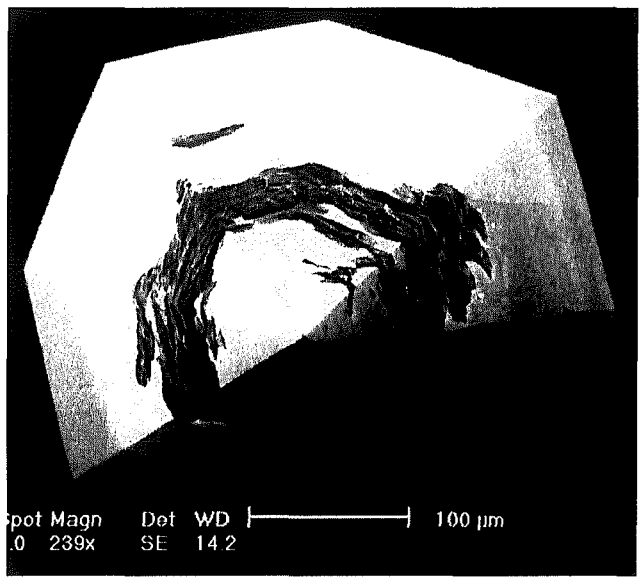

Figure 5.6 A head-on SEM view of a micro needle tested in skin. The skin debris is present only near the tip of the micro needle, and the base of the micro needle is still smooth and shiny.

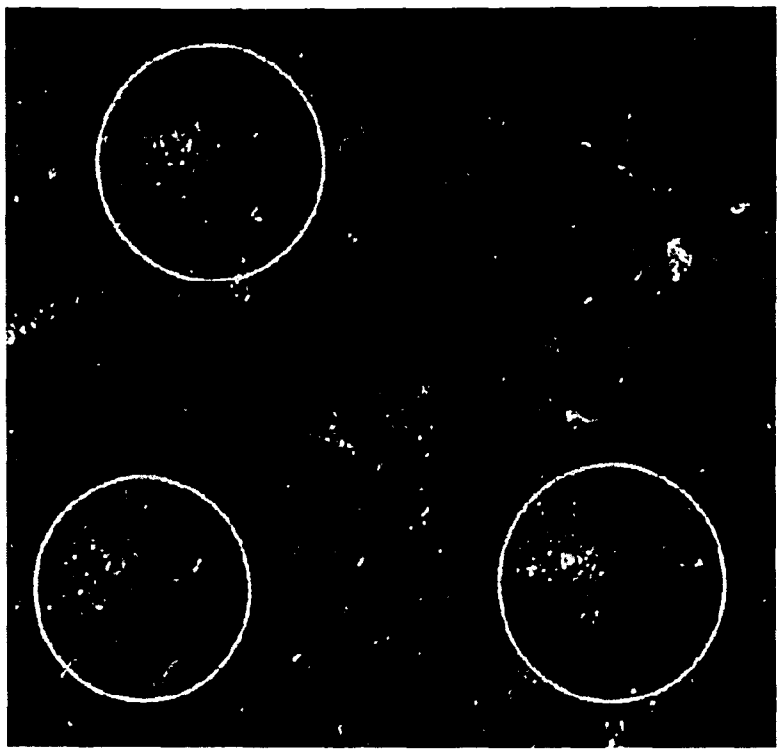

Figure 5.7 A tested Skin sample. Three puncture holes are clearly evident inside the circled zones.

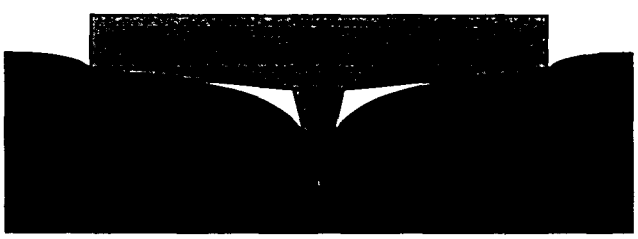

Figure 5.8 A model of elastic deformation of the skin resulting in partial contact with the needle and die. The contact boundaries on the die and needle correspond with the edges of the debris-free regions seen in SEM images after testing.

5.2 Effect of Tip Geometry

The puncture force required to penetrate the skin specimen varies substantially for the three micro needles tested. The variation is attributed to the micro needle tip geometry and its sharpness. Head on SEM pictures of the tips of the three tested micro needles are shown in figure 5.9 at higher magnification. The eight facets of the micro needle do not terminate at the very end of the needle tip, and the degree of failure to do so is different in the three tips. The facets end at different points along the height of the

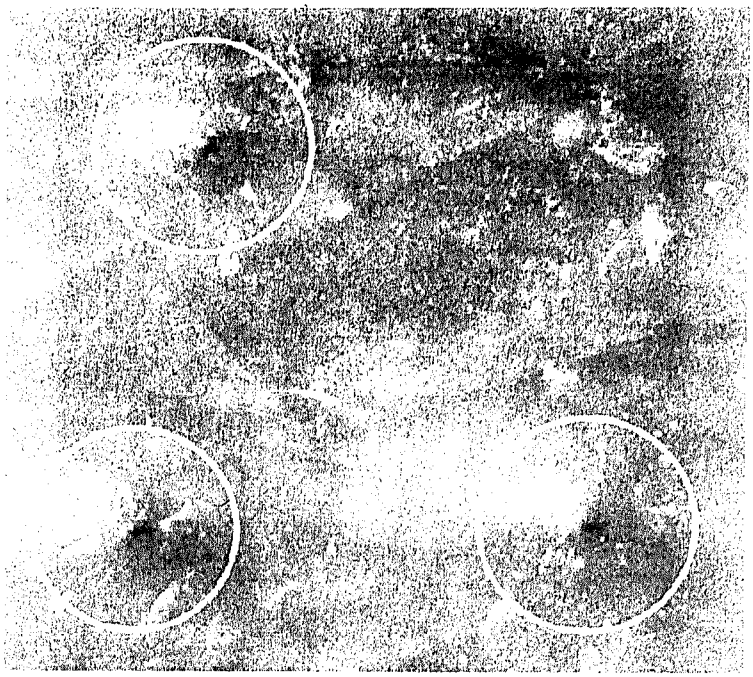

Figure 5.7 A tested Skin sample. Three puncture holes are clearly evident inside the circled zones.

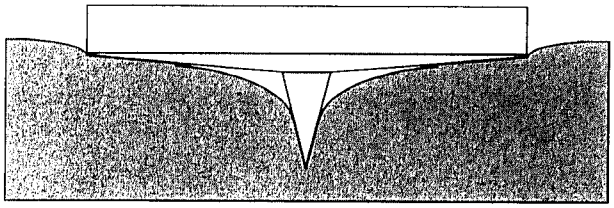

Figure 5.8 A model of elastic deformation of the skin resulting in partial contact with the needle and die. The contact boundaries on the die and needle correspond with the edges of the debris-free regions seen in SEM images after testing.

5.2 Effect of Tip Geometry

The puncture force required to penetrate the skin specimen varies substantially for the three micro needles tested. The variation is attributed to the micro needle tip geometry and its sharpness. Head on SEM pictures of the tips of the three tested micro needles are shown in figure 5.9 at higher magnification. The eight facets of the micro needle do not terminate at the very end of the needle tip, and the degree of failure to do so is different in the three tips. The facets end at different points along the height of the

micro needle near its tip which makes the shape of the micro needles at the tip vary in "sharpness". Considering the dead end of the tip as the origin, successive circles were drawn with increasing diameters of 5,10,20,40 and 60 μm. The degree of geometric sharpness was characterized by the total number of facets that are present at these different distances from the end of the tip. Figure 5.10 shows these values and the variation among the three needle tips is very evident. At the five micron circle around the tip, for example, for the tip of 1F3S only three sides of the micro needle end in this region making it effectively much sharper than the other two needles. This difference can be expected to result in differences in the puncture load, and indeed 1F3S has the lowest puncture load. The other two tips have puncture loads which increase with decreasing sharpness. Six sides of 1G3S end in this 5 micron diameter region leading to the greatest bluntness and hence the highest load would be needed to puncture the skin. Tip 1D3S falls in between the other two in terms of its sharpness and its corresponding puncture load.

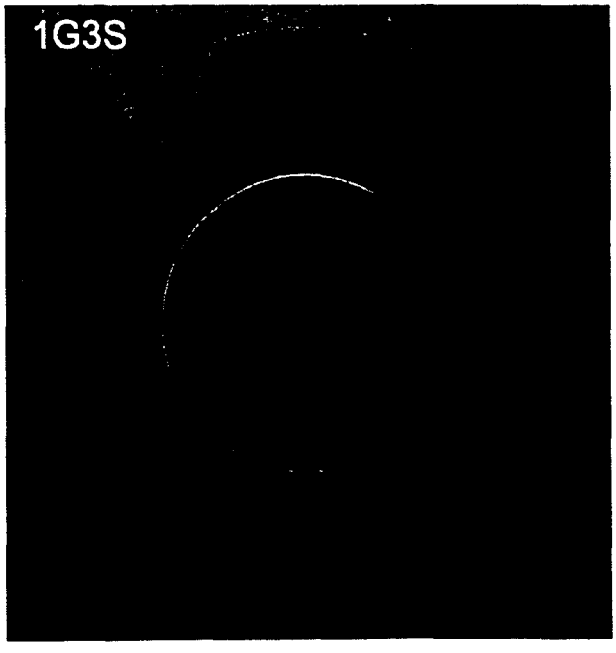

micro needle near its tip which makes the shape of the micro needles at the tip vary in "sharpness". Considering the dead end of the tip as the origin, successive circles were drawn with increasing diameters of 5,10,20,40 and 60 μm. The degree of geometric sharpness was characterized by the total number of facets that are present at these different distances from the end of the tip. Figure 5.10 shows these values and the variation among the three needle tips is very evident. At the five micron circle around the tip, for example, for the tip of 1E3S only three sides of the micro needle end in this region making it effectively much sharper than the other two needles. This difference can be expected to result in differences in the puncture load, and indeed 1E3S has the lowest puncture load. The other two tips have puncture loads which increase with decreasing sharpness. Six sides of 1G3S end in this 5 micron diameter region leading to the greatest bluntness and hence the highest load would be needed to puncture the skin. Tip 1D3S falls in between the other two in terms of its sharpness and its corresponding puncture load.

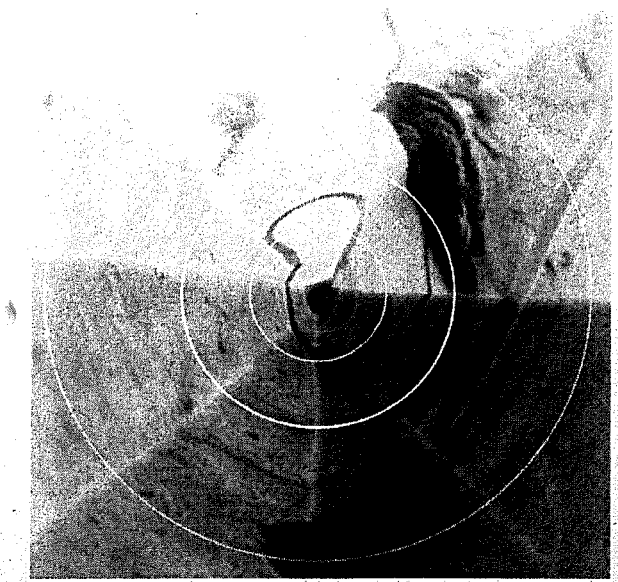

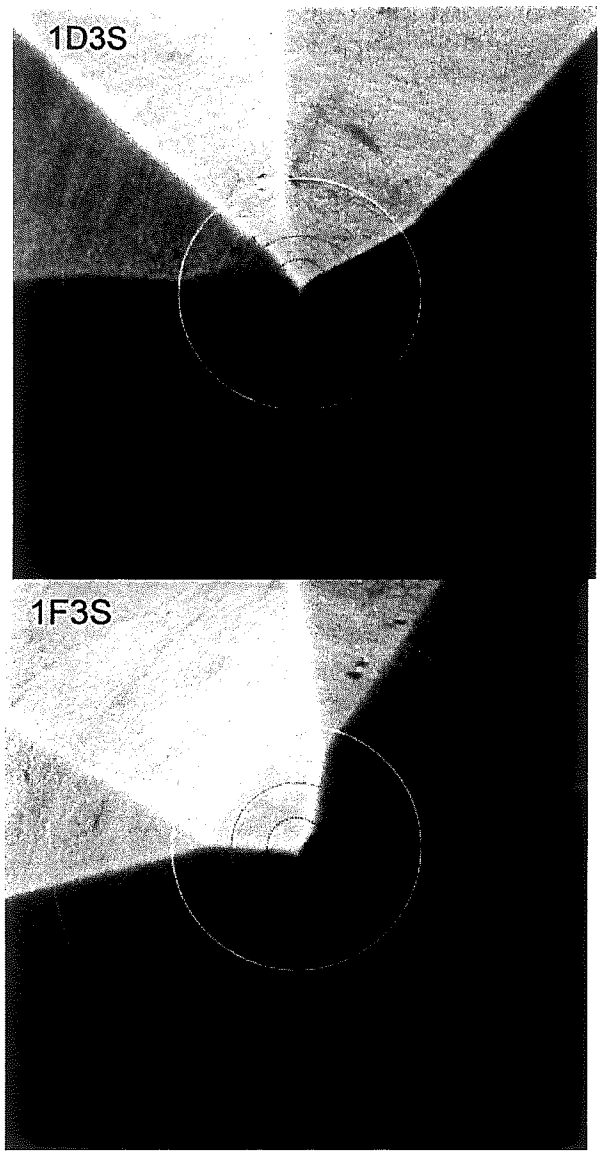

Figure 5.9 Head on view SEM pictures of the tested micro needles at high magnification. Facets end at different heights near the tip of the needle. The circles drawn are of the diameter of 5(pink) 10(green) 20(yellow) and 40(blue) microns. The symmetry of the tip is dissimilar among the needles.

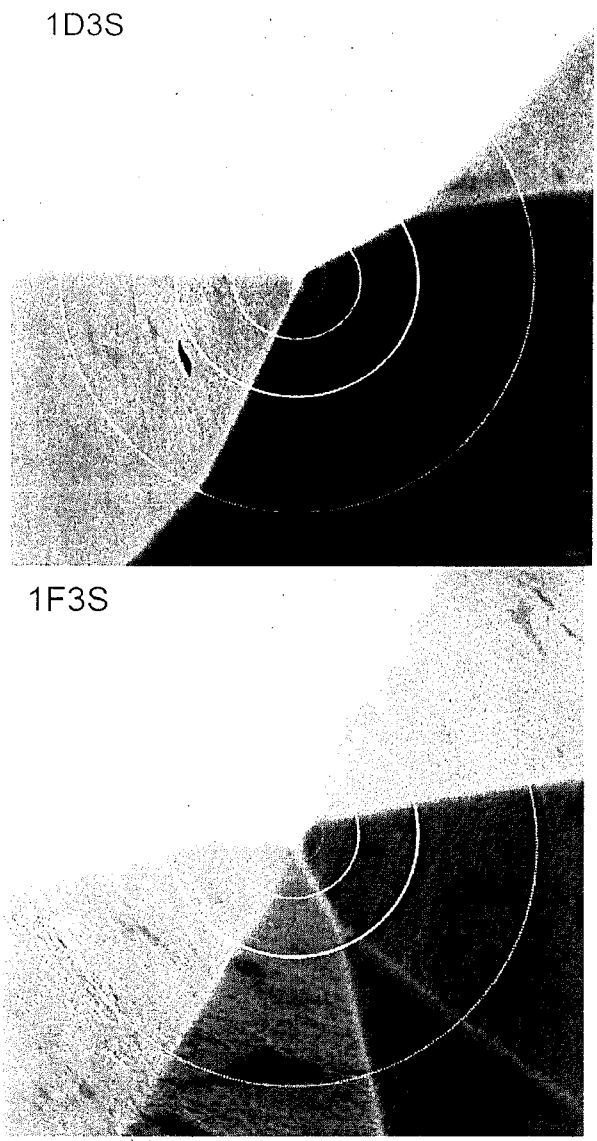

Figure 5.9 Head on view SEM pictures of the tested micro needles at high magnification. Facets end at different heights near the tip of the needle. The circles drawn are of the diameter of 5(pink) 10(green) 20(yellow) and 40(blue) microns. The symmetry of the tip is dissimilar among the needles.

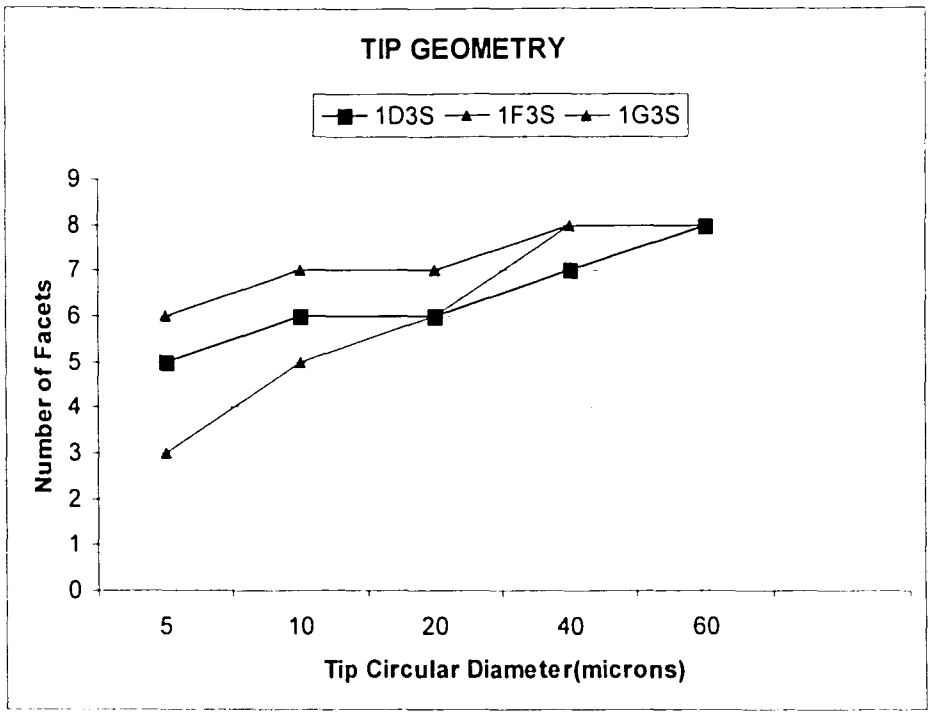

Figure 5.10 The number of facets ending in a circle drawn around the tip.

5.3 Engulfment of Air Gap

The examination of the tested micro needles and the tested skin suggests the possibility that there is an air gap between the skin and the needle die at maximum insertion as sketched in figure 5.8. In an effort to confirm this, video images were captured during penetration of a micro needle into a transparent polymer using an inverted microscope. The needle was advanced at 0.01 mm/s. When the force vs. displacement curve in figure 5.11 is compared with the video images shown in figures 5.12 and 5.13, several important features are apparent. The slope change at 610 mN during penetration happens when the needle die first comes in contact with the material. Only one corner of the needle die initially makes contact with the material. The die

contact zone subsequently spreads around the needle towards the opposite corner of the die, finally leading to an engulfment of air. At full loading, there is clear indication of an air gap visible as lighter zone surrounding the needle. During unloading the jerk at 335 mN is matched to the needle die completely coming out of contact with surface of the material.

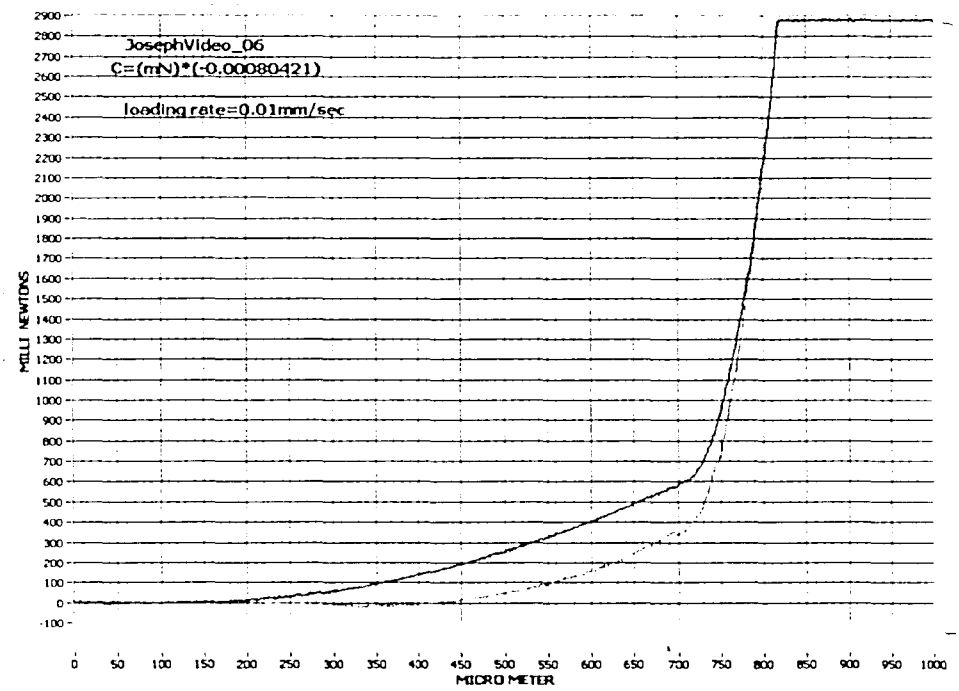

Figure 5.11 A force vs. displacement curve during video indentation. The blue color represents the loading curve and the red represents the unloading curve.

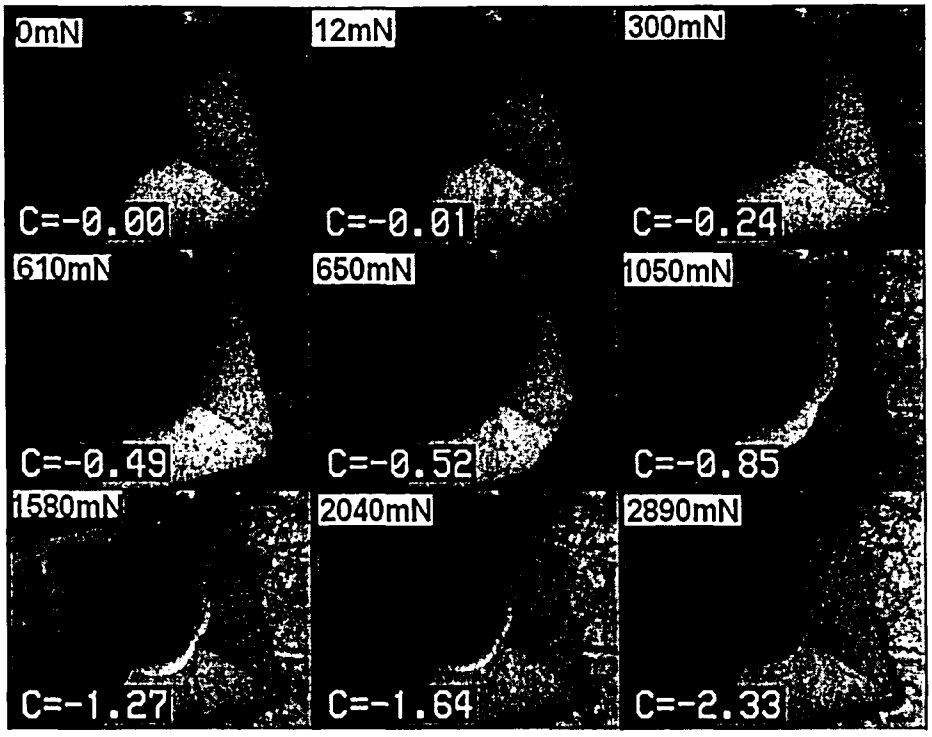

Figure 5.12 The pictures of video indentation during loading. The initial contact of die with the surface of the material is seen at 610 mN. There is a clear evidence of air gap existence between the material and needle die.

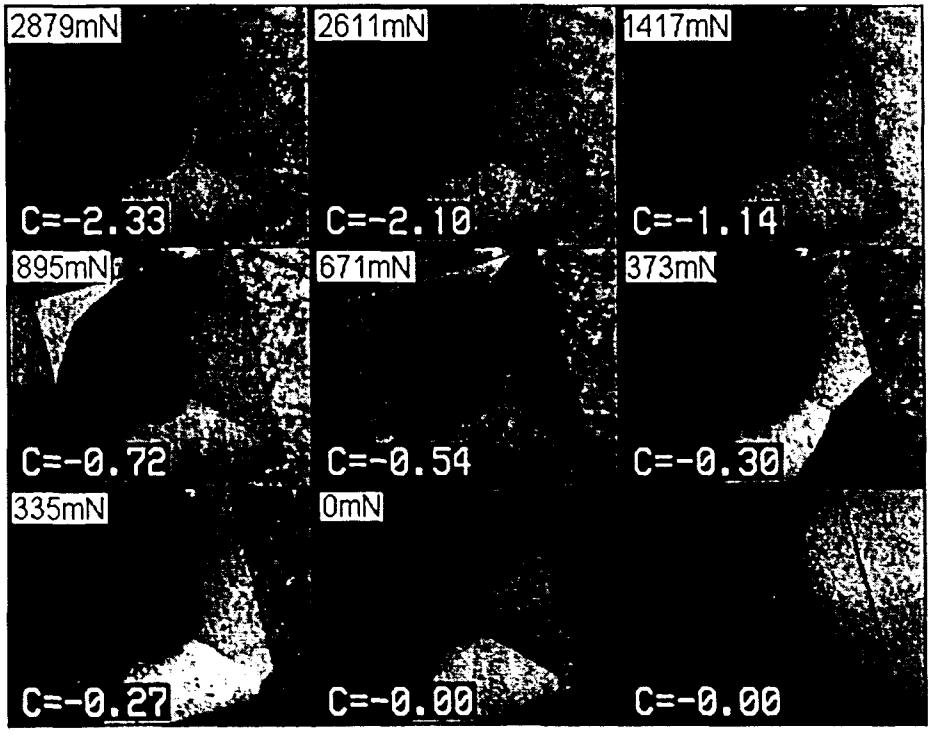

Figure 5.13 The pictures of video indentation during unloading. The die comes out of material contact at 335 mN. There is an imprint of needle die when the needle was completely withdrawn.

5.4 Selection of Synthetic Skin Substitute

To find a possible synthetic substitute for skin, a range of materials with durometer ratings of 20A to 95A were initially selected. These include natural latex, several different formulations of polyurethane, silicones and Formica. These materials were penetrated with the 600 μm long Si micro-needles. Representative results from natural latex (40A), medium-hard polyurethane (60A), firm silicone(50A), and soft silicone(20A) are shown in Figures 5.14-17.

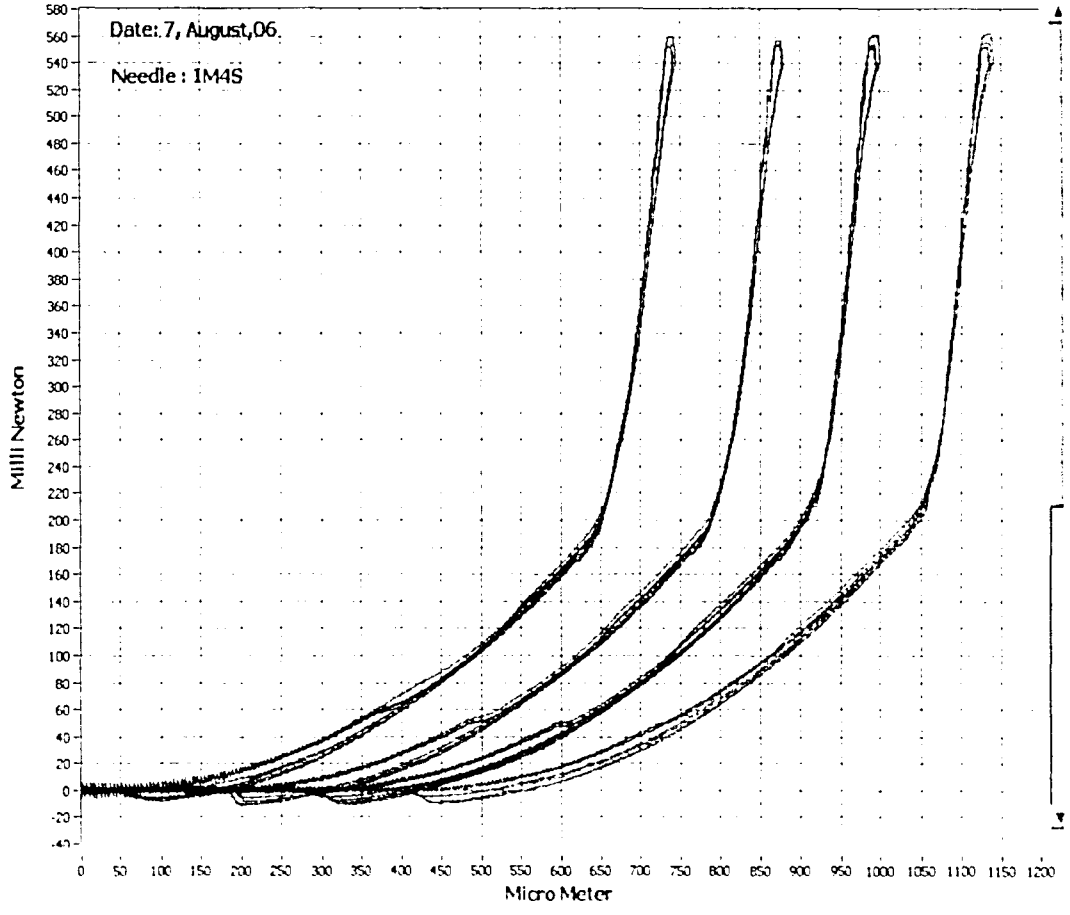

Figure 5.14 Load –displacement curves for four tests performed at different locations in red natural latex (durometer 40A) at 1 mm/s. A single 600 μm long Si needle was used to perform the tests in the order Blue-Red-Green-Pink. Excellent reproducibility is evident. The overlapping loading and unloading curves indicate largely elastic behavior on the part of the latex. The small change in slope between 40mN to 60mN is interesting but not yet understood. The significant increase in slope closer to the end of the loading curves may indicate full insertion of the needle and corresponding contact of the needle base with the polymer. Note that the depth at this slope change correlates well with the expected needle length of 600 μm.

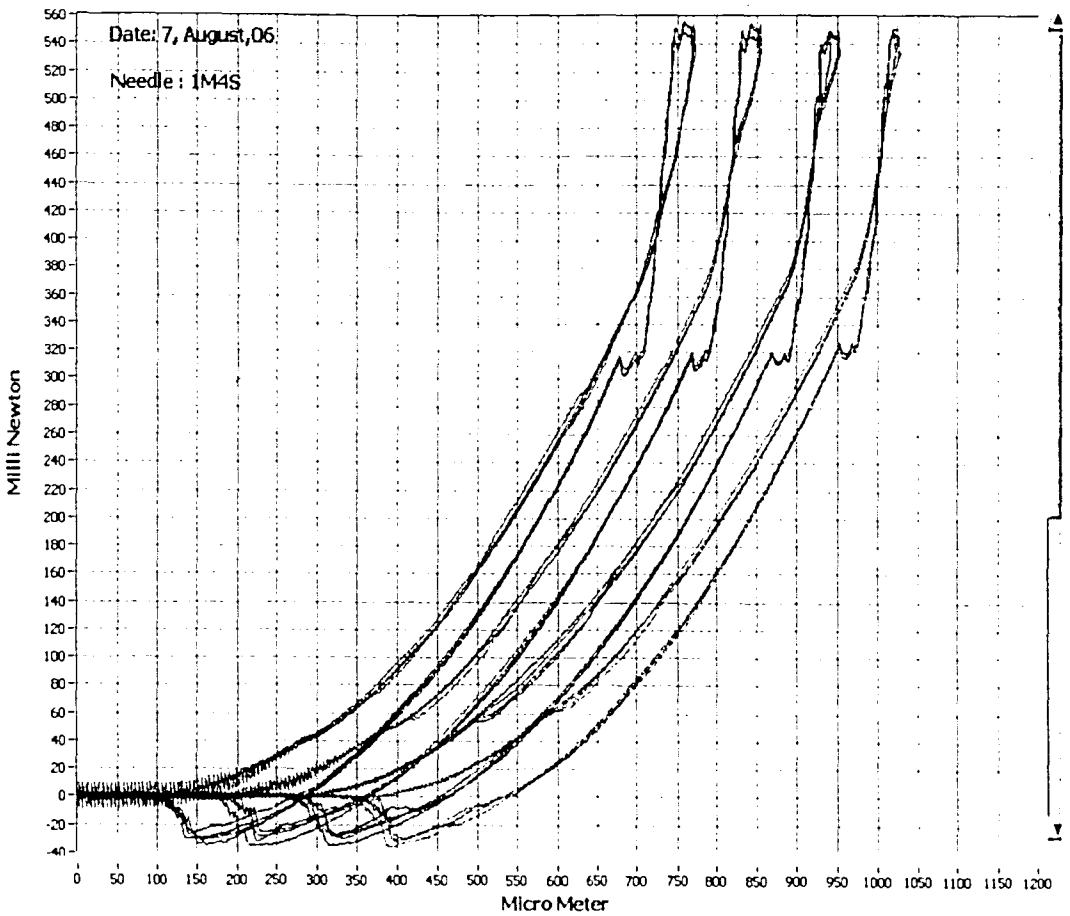

Figure 5.15 Load –displacement curves for four tests performed at different locations in medium-hard polyurethane (durometer 60A) at 1 mm/s. A single 600 μm long Si needle was used to perform the tests in the order Blue-Red-Green-Pink. Excellent reproducibility is evident. The deep cusp and negative values near the end of the unloading segments indicate tension induced by adhesion between the polyurethane and the needle as the needle is withdrawn.

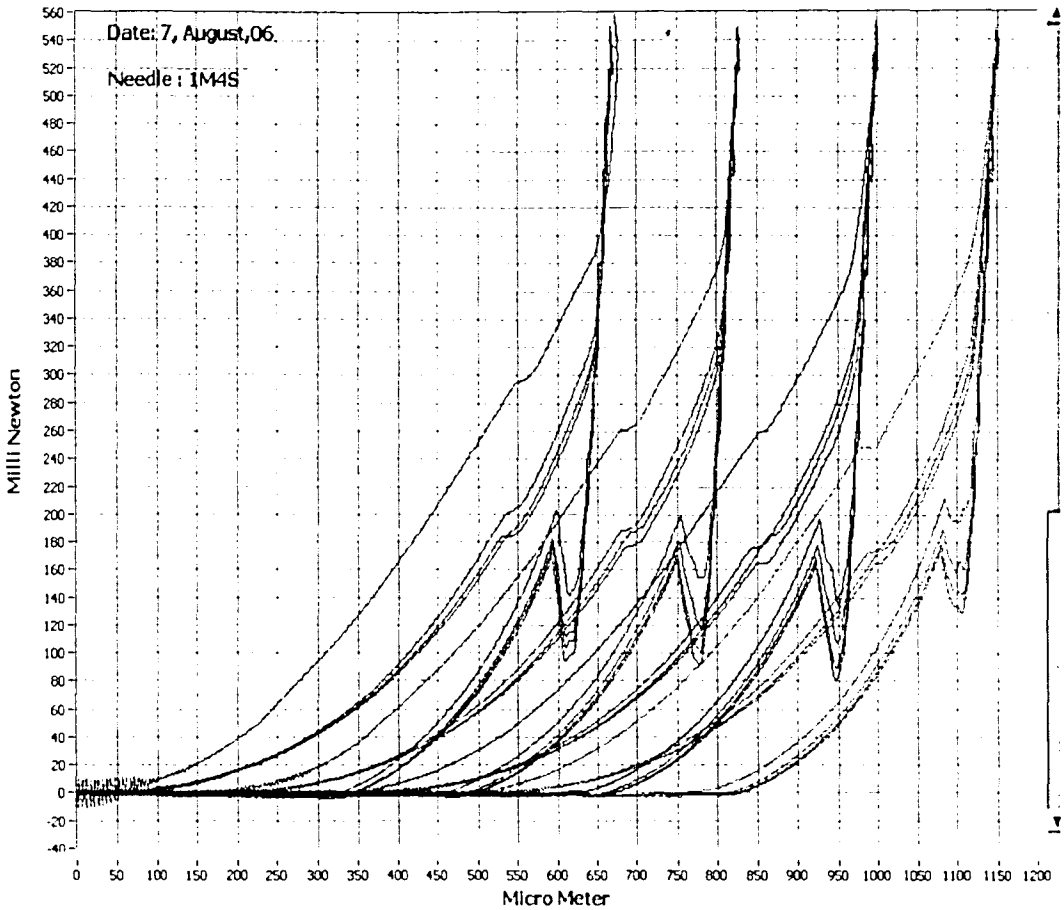

Figure 5.16 Load –displacement curves for four tests performed at different locations in silicone (durometer 50A) at 1 mm/s. A single 600 μm long Si needle was used to perform the tests in the order Blue-Red-Green-Pink. Excellent reproducibility is evident. The sudden spur in the load during unloading indicates the adhesion of needle die with the silicone.

Comparison of behavior of the multiple penetrations of single needle in skin (figure 5.5) and different synthetic materials(5.14-17) clearly indicates that the force vs. displacement curves in skin and in silicone (figures 5.16 and 5.17) are very similar in many respects. The elastic deformation before puncture and the puncture event during loading are both very evident in the first penetration only for these materials, and are not present in the subsequent penetrations.

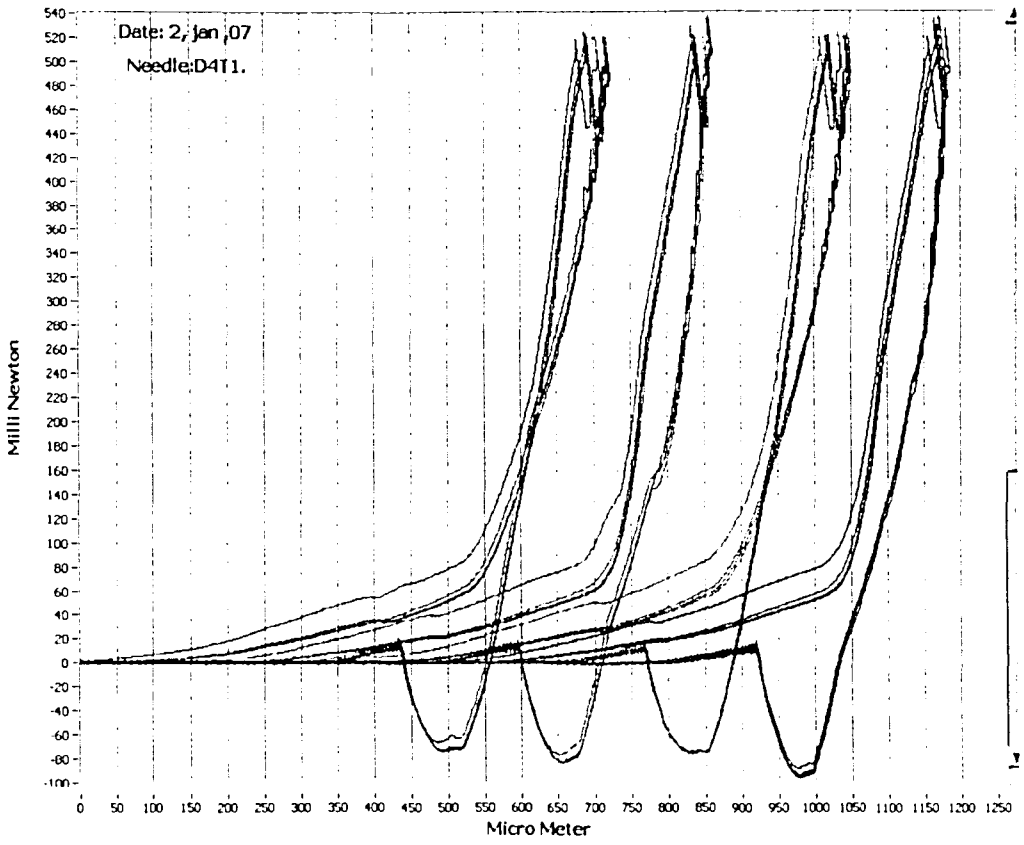

Figure 5.17 Load –displacement curves for four tests performed at different locations in silicone (durometer 20A) at 1 mm/s. A single 600 μm long Si needle was used to perform the tests in the order Blue-Red-Green-Black. Excellent reproducibility is evident. The sudden spur in the load during unloading indicates the adhesion of needle die with the silicone.

Tables summarizing the Durometer hardness of living skin (based on literature values) and each polymer tested, as well as the puncture force measured for each material tested, are shown below. In Table 5.2, it can be seen that the polymers range from 1 to 4 times harder than normal skin as measured by the Shore A test, a blunt deformation test. While the Shore A hardness is a useful quantity, the measured hardness during penetration with a sharp needle is more relevant to the current research tests. Hence hardness was calculated following the usual convention: hardness is defined as load divided by projected contact area as shown in figure 5.18.

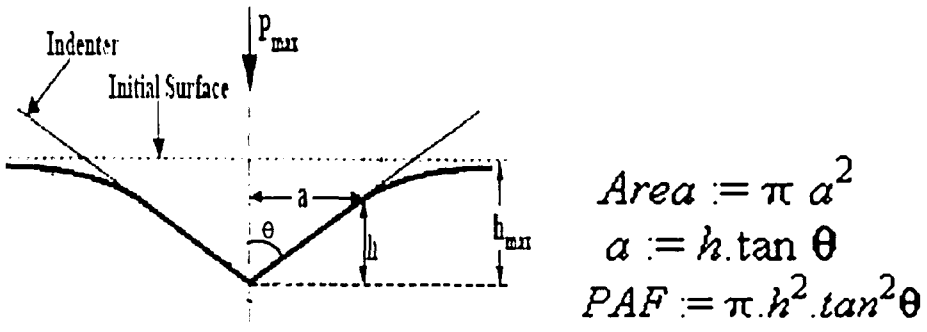

Figure 5.18 An indenter approximated as a cone. The projected area function (PAF) is calculated as a function of needle height (h) and semi-cone angle(θ)

As the needle shape is fairly consistent along its height, the choice of load at which the contact area is determined should not affect the resulting hardness value as long as the measurement is consistently made in the elastic regime. Hence the contact area was calculated at a load which is lower than the average puncture force of the needles when penetrated into skin. As discussed in section 5.1, the average puncture force of the needle in skin was found to be 52 mN. Therefore the contact area was calculated at 40 mN for each material, based on an idealized conical needle with a half angle (θ) of 20 degrees.

The measured hardness values are presented in Table 5.3. The tested skin is cadaver skin; the comparison with living skin is not known. It is assumed that the behavior is similar since the major structural elements are retained in the cadaver skin. It can be seen that the sharp indenter results show even larger differences between the polymers and cadaver skin than the durometer values quoted in the literature for normal skin as indicated in Table 5.2. Among the polymers

Material	Hardness Shore A	Polymer / Normal skin Shore A hardness ratio	Polymer / Scarred skin Shore A hardness ratio
Normal skin	20	1	
Scarred skin	45	2.3	1
20A Silicone	20	1	0.4
30A Silicone	30	1.5	0.6
35A White latex	35	1.8	0.8
40A Red latex	40	2.0	0.9
40A polyurethane	40	2.0	0.9
50A silicone	50	2.5	1.1
60A polyurethane	60	3.0	1.3
80A polyurethane	80	4.0	1.8

Table 5.2 Shore A hardness values for living human skin and for a variety of elastomeric polymers. All values are extracted from published literature.

Material	P. Depth (um)	Projected Area Function (um^2)	Hardness (N/um^2)	Relative Hardness	Puncture Force (mN)	Material /Cadaver Skin puncture force ratio
CADAVER SKIN	433	78355	0.51	1	52	
20A Silicone	340	48105	0.83	1.6	45	**0.87**
30A Silicone	237	23304	1.71	3.3	Unclear	
35A Latex	240	23956	1.66	3.2	Unclear	
40A Latex	230	22001	1.81	3.5	Unclear	
40A Poly urethane	200	16636	2.40	4.6	Unclear	
50A Silicone	170	12020	3.32	6.4	266	**5.1**
60A Poly urethane	160	10647	3.75	7.3	Unclear	
80A Poly urethane	110	5032	7.94	15.4	428	**8.2**

Table 5.3 Measured penetration hardness and puncture force values for human cadaver skin and for a variety of elastomeric polymers. All values were determined at 40 mN.

listed in table 5.3, the polymers which exhibit clear puncture force are therefore considered as good candidates to substitute for skin. The materials such as 35A latex, 40A latex, and 60A polyurethane display no distinct puncture events and hence are rejected.

The 20A silicone exhibited a puncture force of 45±8 mN and a material/cadaver skin puncture ratio of 0.87. Besides, the behavior of the force vs. needle displacement curves in 20A as shown in figure 5.17 is similar to what was observed in cadaver skin, as tested four times with a single needle although the 2^{nd}, 3^{rd} and 4^{th} penetration forces are much higher than for skin. Hence, 20A silicone is considered as a material of choice to substitute for skin.

As a safety factor during micro needle reliability testing, a polymer that has a hardness that is several times that of normal skin is required, with a value at least equal to that of heavily scarred skin (with which the needles are not intended to be used). It is also desired to have a polymer that displays a clear puncture event, and which can be punctured at a load level that ensures puncture of all needles in a 3x3 array at a maximum force of approximately 9600 mN (2.1 lbs) - the safe limit of the 1 kg load cell. The puncture event in the 80A polyurethane is difficult to discern, but not impossible (as shown in figure 5.19). However, the hardness and resistance of the 80A to puncture is so high that the penetration of all nine needles in a 3x3 array cannot be ensured. Thus the 80A is rejected, and the 50A silicone is chosen as the model polymer for needle reliability testing. As seen in Table 5.3, it has a safety factor of 6.4 for penetration hardness and 5.1 for puncture load as compared to the average behavior of normal cadaver skin. The 50A silicone polymer shows good consistency, with an average

puncture load of 266 ±20 mN and die contact load of 378 ±10 mN, as tested four times with one single needle. The puncture load uncertainty is only 7.5%, which compares favorably to the worst-case 31% measured for the cadaver skin(with three different needles). This supports the conclusion that the polymer serves as a useful substitute for skin during micro needle reliability testing in normal force penetration.

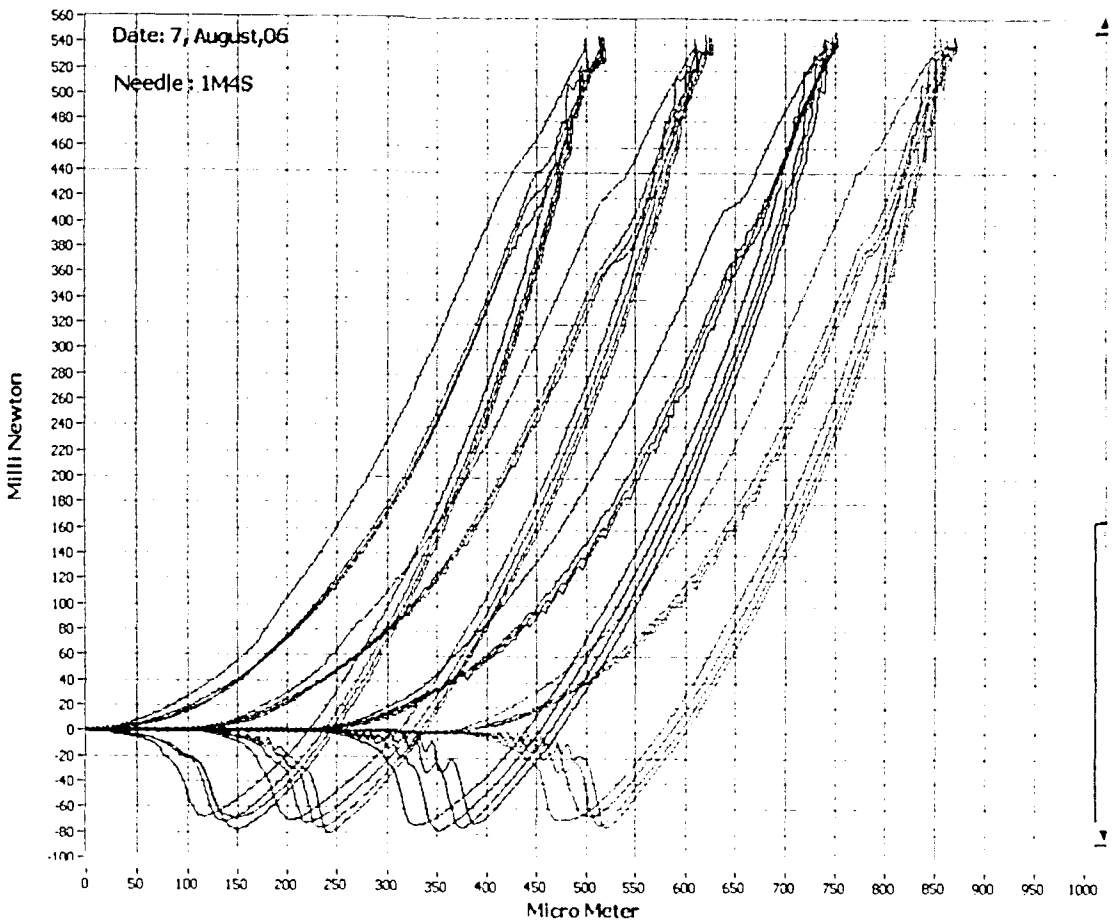

Figure 5.19 Load –displacement curves for four tests performed at different locations in hard polyurethane (durometer 80A) at 1 mm/s. A single 600 μm long Si needle was used to perform the tests in the order Blue-Red-Green-Pink. The puncture force is difficult to discern. The deep cusp and negative values near the end of the unloading segments indicate tension induced by adhesion between the polyurethane and the needle as the needle is withdrawn.

5.5 Reliability of Silicon Micro Needles

All tests were performed using the 50A silicone with only one penetration into the material. Results of tested needles are given in Table 5.4, along with details of the needle

state prior to testing, the maximum load during testing, and the total needle travel relative to the surface of the sample. No fracture resulting from testing in 50A silicone was found in any needle, regardless of starting state. SEM images of one needle array in Lot 1 (2A1A) are given in Figure 5.20, before and after testing. Some needles had minor tip damage when they arrived at Lehigh, presumably from the gel pack hand-packing process. These needles also suffered no visible change after testing, as shown in Figure 5.21, despite the preexisting non-ideal tip shape.

Lehigh ID	Apogee ID	Maximum Load(mN)	Needle displacement relative to sample surface(um)	Existence of prior tip damage (Y/N)	Fracture from Testing (Y/N)
2A1S	A6-1-1(top)	9600	930	NO	NO
2B1S	A6-1-1(left)	9600	880	NO	NO
2C1S	A6-1-1(bottom)	9500	970	NO	NO
2D1S	A6-1-1(right)	9600	960	NO	NO
2M1S	A6-1-1(middle)	9650	920	NO	NO
2A1A	A6-1-1(top)	9400	700	NO	NO
2B1A	A6-1-1(left)	9300	700	YES	NO
2C1A	A6-1-1(bottom)	9300	730	NO	NO
2D1A	A6-1-1(right)	9300	710	YES	NO
2M1A	A6-1-1(middle)	9400	710	YES	NO
3A1S	A6-1-2(top)	9600	920	NO	NO
3B1S	A6-1-2(left)	9500	920	NO	NO
3C1S	A6-1-2(bottom)	9500	970	NO	NO
3D1S	A6-1-2(right)	9600	910	NO	NO
3M1S	A6-1-2(middle)	9600	910	NO	NO
3A1A	A6-1-2(top)	9400	700	NO	NO
3B1A	A6-1-2(left)	9400	690	NO	NO
3C1A	A6-1-2(bottom)	9300	700	YES	NO
3D1A	A6-1-2(right)	9300	650	NO	NO

3M1A	A6-1-2(middle)	9300	700	NO	NO
4RS	A6-1-3 (R)	9400	940	NO	NO
4TS	A6-1-3 (T)	9400	940	NO	NO
4LS	A6-1-3 (L)	9400	920	NO	NO
4BS	A6-1-3 (B)	9500	960	NO	NO
4CS	A6-1-3 (C)	9500	920	YES	NO
4RA	A6-1-3 (R)	9300	660	NO	NO
4TA	A6-1-3 (T)	9300	730	NO	NO
4LA	A6-1-3 (L)	9400	730	NO	NO
4BA	A6-1-3 (B)	9500	710	NO	NO
4CA	A6-1-3 (C)	9500	700	YES	NO
5RS	A6-2-3 (R)	9500	910	NO	NO
5TS	A6-2-3 (T)	9500	940	NO	NO
5LS	A6-2-3 (L)	9400	910	NO	NO
5BS	A6-2-3 (B)	9500	950	NO	NO
5CS	A6-2-3 (C)	9500	980	NO	NO
5RA	A6-2-3 (R)	9400	730	NO	NO
5TA	A6-2-3 (T)	9400	745	NO	NO
5LA	A6-2-3 (L)	9300	720	NO	NO
5BA	A6-2-3 (B)	9500	760	NO	NO
5CA	A6-2-3 (C)	9400	725	NO	NO
6RS	A6-2-4 (R)	9500	860	NO	NO
6TS	A6-2-4 (T)	9400	880	NO	NO
6LS	A6-2-4 (L)	9400	960	NO	NO
6BS	A6-2-4 (B)	9400	950	NO	NO
6CS	A6-2-4 (C)	9300	910	NO	NO
6RA	A6-2-4 (R)	9500	770	NO	NO
6TA	A6-2-4 (T)	9400	750	NO	NO
6LA	A6-2-4 (L)	9300	740	YES	NO
6BA	A6-2-4 (B)	9500	740	NO	NO
6CA	A6-2-4 (C)	9400	730	NO	NO

Table 5.4 Reliability results from normal-force testing of single needles and arrays.

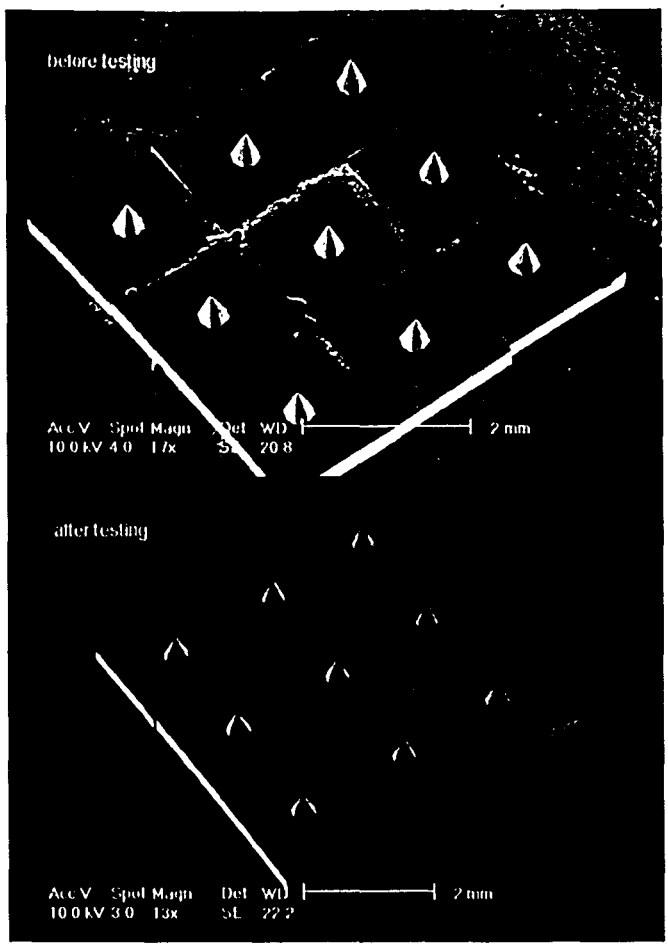

Figure 5.20 Array 2A1A, from Lot 1, is shown before and after testing in 50A silicone. Small amounts of conductive epoxy are visible between the dies. As the epoxy is fully cured before testing, it is not expected to play any role in the penetration and retraction behavior.

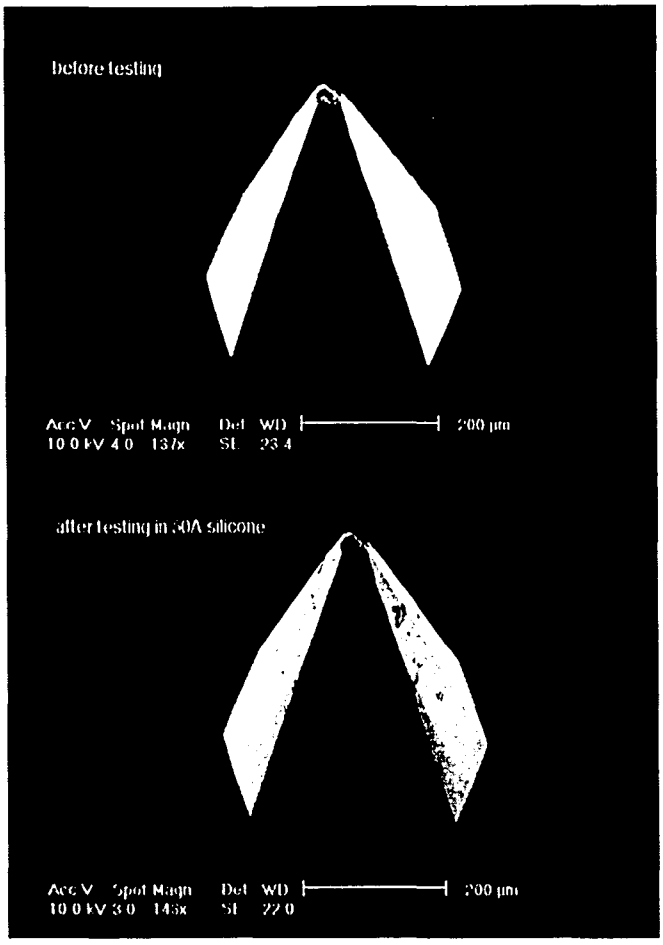

Figure 5.21 Needles with preexisting damage, most likely resulting from handling. No additional damage was visible after testing, but there are many particles clinging to the surface as a result of penetration into the silicone. The particles are typical of all needles after testing, and are not related to the prior tip damage. (Array 2D1A, needle 4).

5.6 Contact Area Measurement

Drug molecules can be introduced into the body in a variety of ways, but the effectiveness of drug therapy depends on the rate and extent to which the drug molecules can move through the tissue structure to reach their site of action. Assuming that the drug delivery needles are to be coated with drug molecules then the drug dose reaching the blood circulation will be governed by the amount of surface area of the coated needle penetrated into the skin. Hence the estimation of exact penetrated contact area of silicon micro needle inside the material is very critical to calculate the dose of a drug as the rate of diffusion crucially depends on the contact area. the two techniques that were

developed in this research work to estimate the surface contact area of the needle are presented below.

A representative picture of a needle tested in 20A silicone using the nail polish technique is shown in the figure 5.22. While penetrating, the nail polish is sheared to form a boundary layer due to intimate frictional contact of the needle with the 20A silicone material. The important feature of penetration depth is the distance between the tip of the needle and the sheared nail polish boundary which is very clearly seen on the needle in figure 5.22a. The presence of the unsheared nail polish area matches the hypothesis that there is a gap between the needle and the material due to the elastic deformation of material.

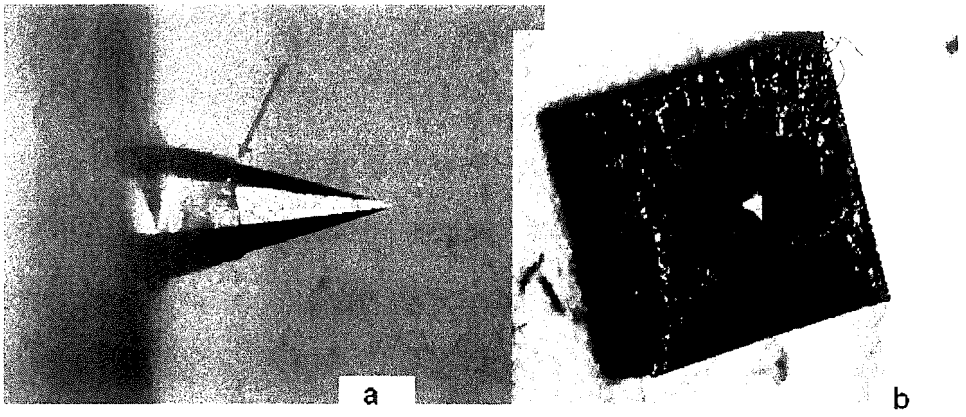

Figure 5.22 a) Needle tested in 20A polymer coated with a thin layer of nail polish. The needle was advanced into the material to a fixed distance of 500 microns from initial contact surface at the rate of 1.0 mm/s using 50g load cell. The sheared boundary of nail polish is very evident on the needle revealing the contact area of the needle with the punctured material. The needle die/stub and sheared boundary are marked with arrows b) shows the head on view of the tested needle which further supports the discussion of an air gap at the base of the needle due to deformation of the polymer around the needle as sketched in fig 5.8.

It is worth noting that the distance between the die/stub interface and the tip of the needle(d1) was found to be 940 microns in SEM images. The distance from the sheared nail polish boundary to the tip of the needle(d2) was dependant on the predetermined

needle advance from the surface of the material. The ratio of d2 to d1 times the original total length of a micro needle (940 microns) was considered to be the actual length of needle inside the penetrated material. Then the estimated contact area of the needle can be obtained by using cone approximation to model the slanting surface area. The percentage of the needle inside the material is shown in figure 5.23.

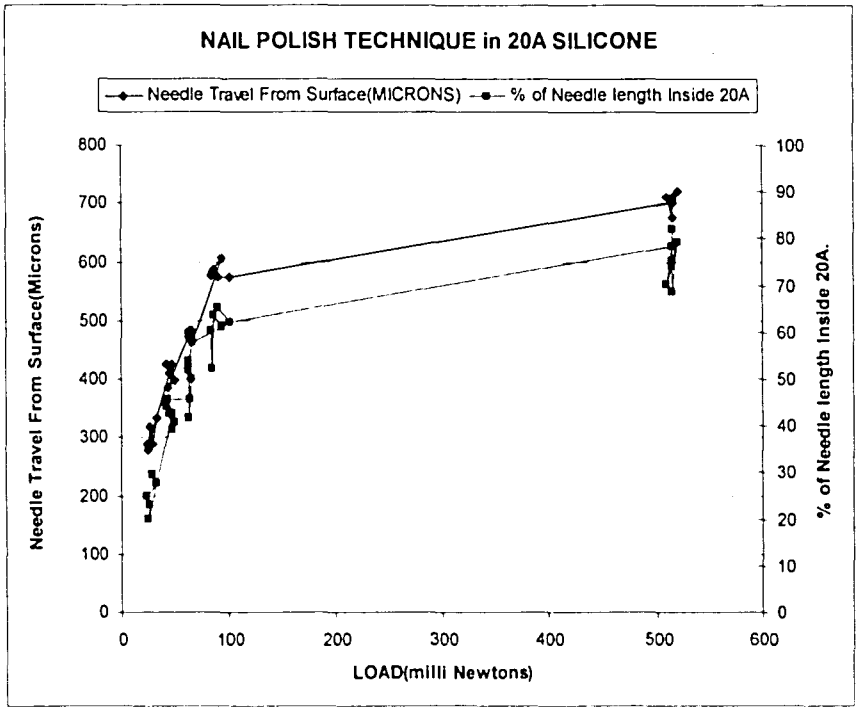

Figure 5.23 The percentage height of the needle inside the material after penetration into it.

Although the contact area measurements using the organic nail polish technique are fairly consistent, it critically depends on the fast drying time of the nail polish. The very short drying time makes the experiments difficult. This significant time constraint can be avoided by using thin inorganic aluminum foil (25 micron thickness). The aluminum sheet was placed on the mounted 20A silicone and the needle was advanced at 1 mm/s. The optical image of the aluminum sheet tested at full loading of 50g load cell is shown in figure 5.24. The absence of aluminum sheet in the indented area is interesting to

explore, and a hole in the center of this area implies the successful penetration of the micro needle.

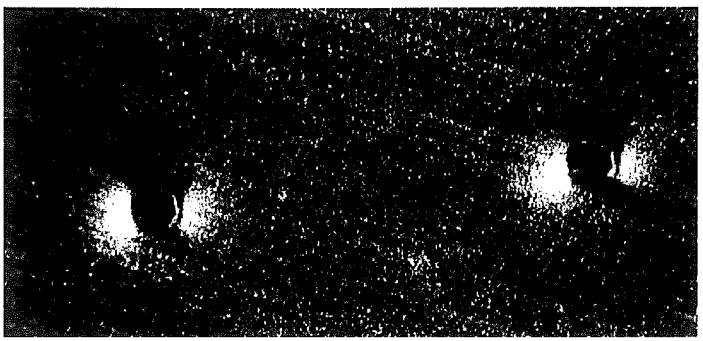

Figure 5.24 An optical image of two indentation imprints of a needle in the aluminum foil over 20A silicone at full loading in 50 g load cell. The 20A silicone shows through the center of both holes.

The SEM image of the indented area is shown in the figure 5.25, and the opening of the aluminum foil is similar to the octagonal shape of the needle. The tearing of the aluminum has occurred at the four corners of the needle which have narrow angles. During loading, the micro needle has deformed and cut the aluminum sheet as well as the 20A silicone. But during unloading, the elastic recovery of 20A silicone alone has occurred which has probably dragged away the deformed aluminum sheet from the penetration area. The complete recovery of the 20A is also likely halted by aluminum as four tearing spots act like a grip. It is expected that the deformed aluminum might have rolled under between the 20A and the rest of the aluminum sheet. The penetration hole is an amazing shape like flower petals and the shape of the hole depend on the tip of the needle. The concentric circles around the central hole suggests that there is layer by layer penetration of the needle into the 20A, however there is no evidence of this in the load cell measurements.

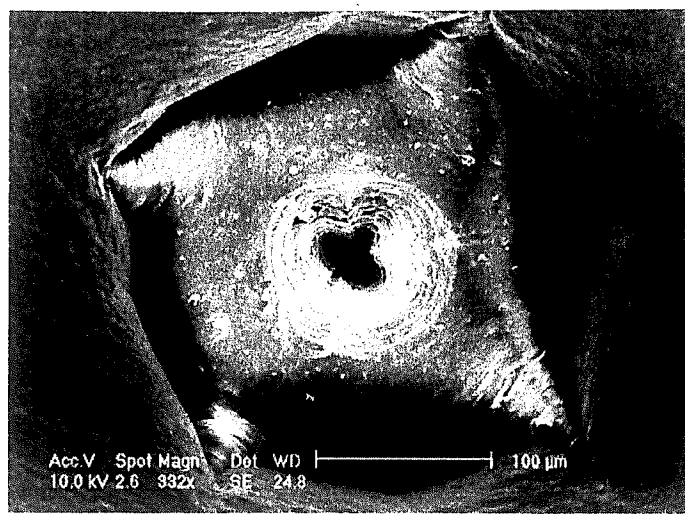

Figure 5.25 The SEM picture of the tested aluminum foil in 20A silicone.

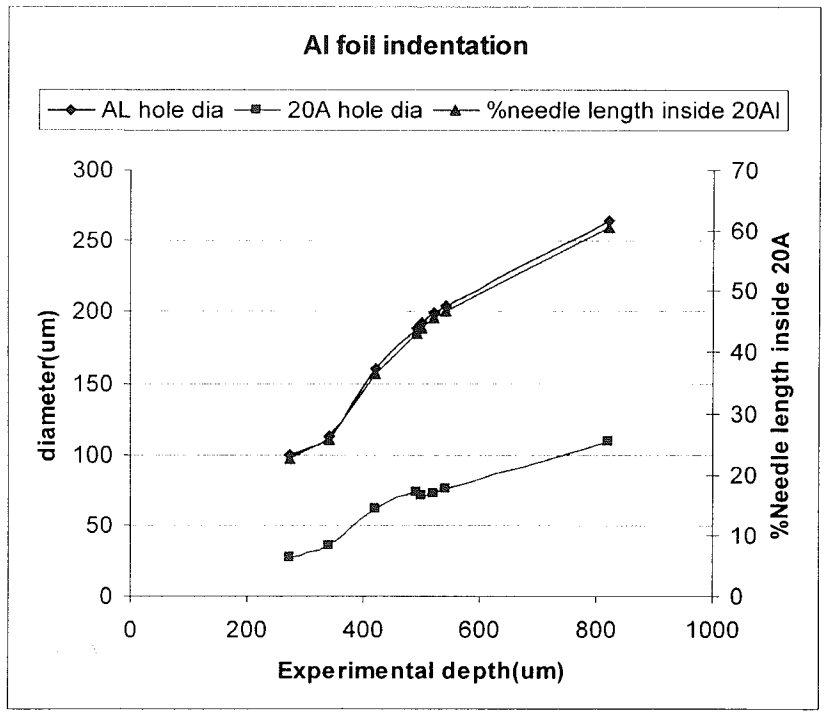

Figure 5.26 The diameter of the hole vs. the depth of needle advanced. Even at full loading of 50g load cell only 60% of total length of needle is inside the 20A at the depth of 820 microns needle advance from the surface of the material. This further bolsters the discussion of an air gap between the needle and the 20A polymer.

The diameter of the holes in aluminum and in 20A silicone created by the needle penetration was measured and plotted against the depth of the needle advance as shown in figure 5.26.

5.7 Scaling Factor

As the silicon micro-needles are meant for drug delivery, the desired amount of drug delivered depends on how much of the needle is penetrated into the skin. Also if a transdermal patch is designed to have a array of needles then the penetration depth depends on how much force was applied to the patch. Hence it is important to find the correlation between the number of needles and the force required to penetrate the material.

Several different kinds of arrays were constructed and systematically tested in 20A silicone polymer at 1.0 mm/s using the 1 kg load cell. The penetration load vs depth for each array was compared with the penetration load vs depth of the 3x3 array which was the maximum array size studied. The load values were compared on logarithmic scales.

A set of representative scaling comparisons performed among the arrays is shown in figures 5.27 and 5.28. The mN load values are expressed on a log scale. It is evident that the curves of a particular type of array tested at different locations on the same piece of polymer superimpose nicely.

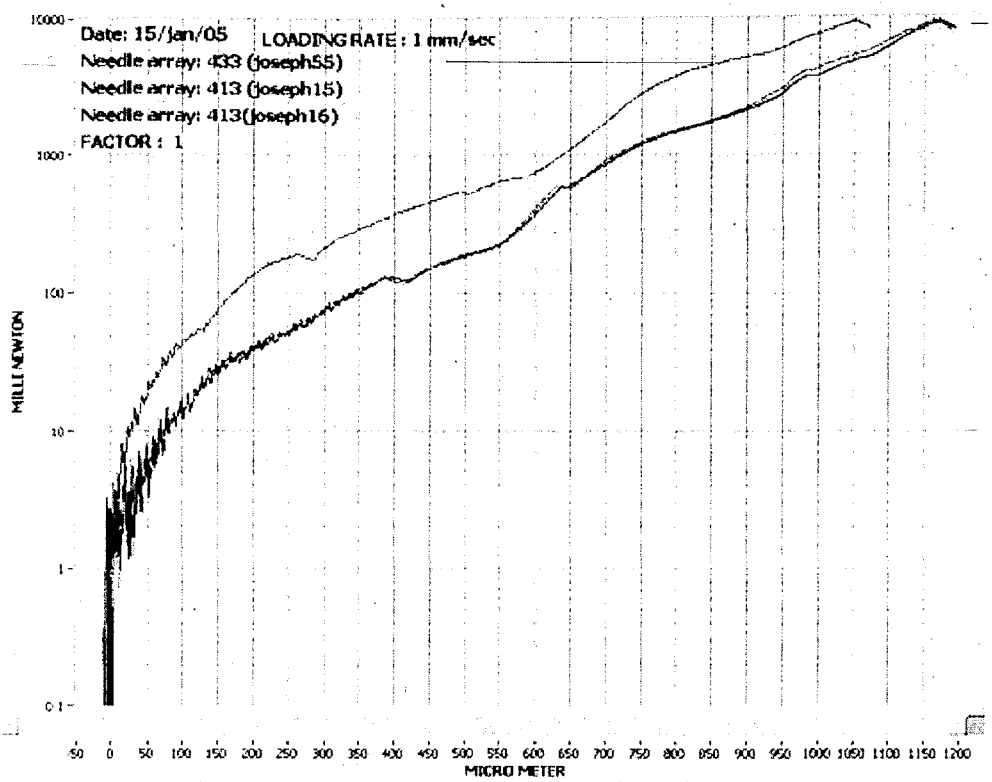

Figure 5.27 The two curves of a single a 1x3 array and one curve of a 3x3 array for comparison on a logarithmic scale. The curves of two tests of a 1x3 array match superbly between themselves. It is also evident that the 3x3 array requires more load than the 1x3 array at any given distance of needle advancement. The label 433 stands for 3x3 array in wafer #4.

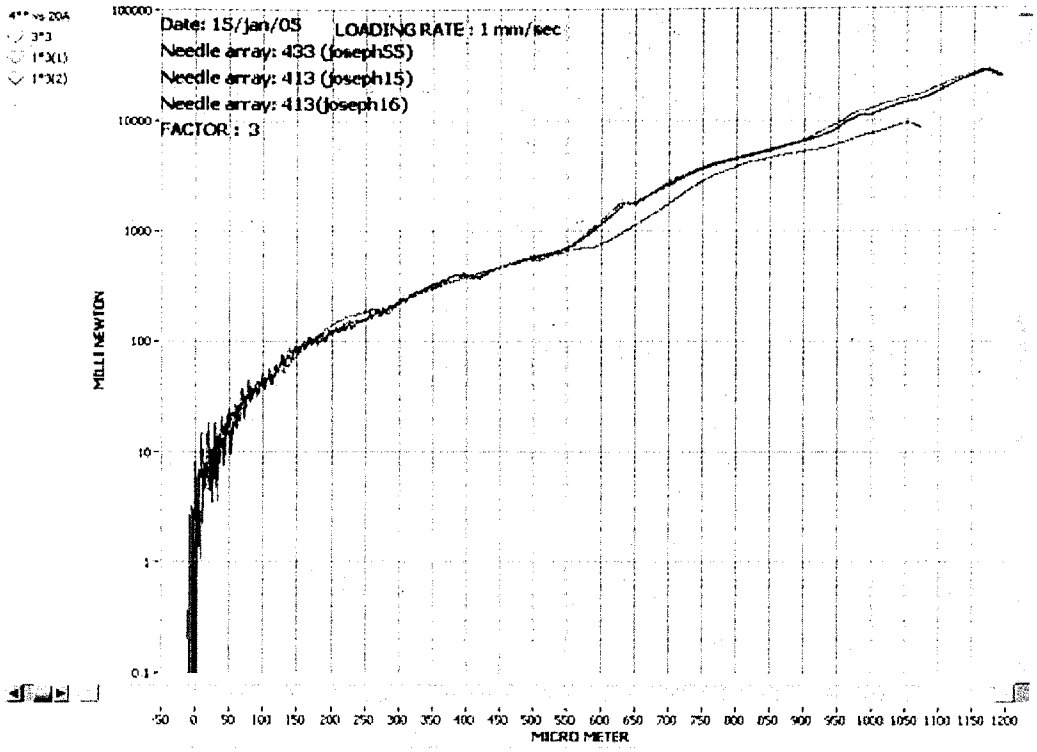

Figure 2.28 Two curves of the same 1x3 array and one curve of the 3x3 array for comparison on logarithmic scale data from figure 2.27. When the 1x3 load values are multiplied by a factor of three they match the load values obtained from the 3x3 array. This clearly indicates a factor of three for an array with three needles to scale with the array of nine needles.

The curves below 600 microns were expected to match best as the needle length is about 600 microns. Any deviation in the curve after 600 microns is basically due to the needle dies and finally the mounting stub coming in contact with the material. The experimental scaling ratio was plotted against the actual needle ratio as shown in figure 5.29. It shows almost perfect linear scaling factor with the needle ratio. This demonstrates that the minimum spacing of the needles required by the current 2 x 2 mm die size is sufficiently large that each needle behaves independent of its neighbors.

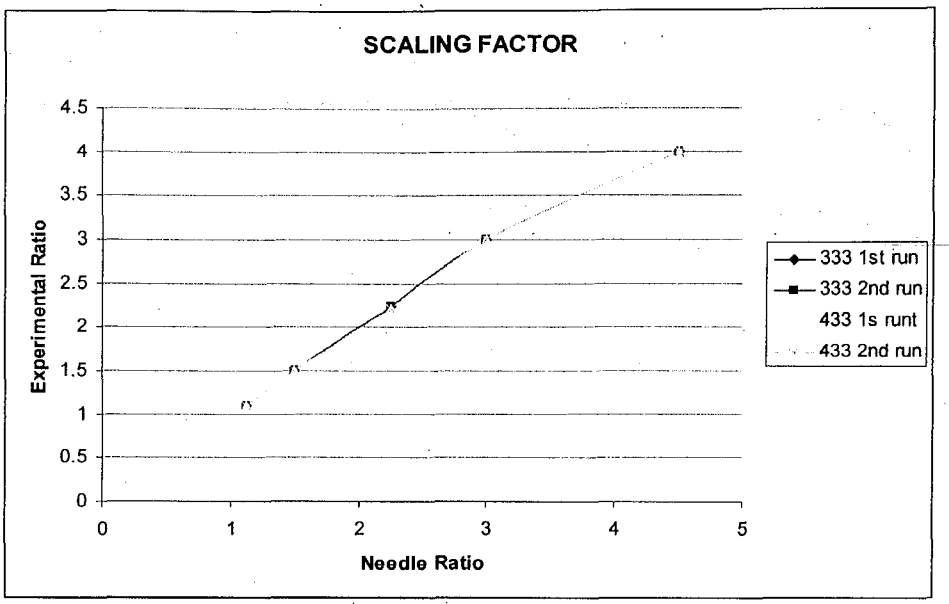

Figure 5.29 The experimental load ratio vs. the needle count ratio. The data fall on a nearly straight line which implies that the penetration force depends linearly on the number of needles in the array.

6. CONCLUSIONS

Penetration experiments have been performed on human cadaver skin and different elastomeric polymers with silicon micro needles. The experiments in human cadaver skin revealed an average puncture force of 52±22 mN and a large elastic deformation of the skin before puncture. The puncture force was significantly consistent for a given needle in the skin but varied substantially for different needles. The variation in the puncture force for different needles was due to different degrees of the sharpness of the needle tip geometry. Among the different elastomeric polymers tested, 20A silicone was selected as the material of choice as a direct synthetic skin substitute. The 20A silicone displayed similar force vs. displacement behavior to that of the tested skin. It also exhibited a distinct puncture event with a puncture force of 45±8 mN. For testing the needle reliability, 50A silicone polymer was found to be a good candidate that displayed a distinct puncture event but at a load about 6 times greater than cadaver skin. The advantage of using these silicones in penetration experiments is that it is relatively straightforward to explore a range of mechanical properties of the silicon micro needle penetration and hence devise improvements in the micro needle design without the complications and cost of skin experiments.

It was also seen that there is a strong possibility of an air gap entrapped between the skin and the needle die around the base of the needle. This has been established by the contact area measurement using a nail polish technique for a single needle inserted into 20A at different positions which was fairly consistent. An aluminum foil test also indicated an air gap as did video evidence of penetration into a transparent silicone. Further exploration of these tests will be very beneficial.

6.1 Future work

Although this research provided initial insight into silicon micro needle penetration in skin, a great deal of work will be needed to gain a thorough understanding of the processes and the implications of these for transdermal drug delivery. Some of them are:

1) Modeling the shape of the deformation of skin and polymer as the needle penetrates into them and ultimately punctures them. This modeling should also include the frictional and cutting forces of the needle in the post puncture period.

2) Further experiments to determine the modulus of the skin with a flat punch or ball and creep recovery tests to understand the visco-elastic behavior of skin.

3) Further experiments to verify the deformation of skin.

4). Further exploration of tip geometry and its implications for puncture.

LIST OF REFERENCES

1. Amy C. Richards Rayson, Rebecca S. Shawgo, Audrey M. Johnson, Nolan T. Flynn, Yawen Li, Michael J. Cima, and Robert Langer, "A BioMEMS Review: MEMS Technology for Physiologically Integrated Devices", Proceedings of the IEEE, Vol. 92, No. 1, January 2004, Pages 6 - 21.

2. Gabriela Voskerician, Matthew S. Shive, Rebecca S. Shawgo, Horst von Recum,James M. Anderson, Michael J. Cima, Robert Langer, "Biocompatibility and biofouling of MEMS drug delivery devices", Biomaterials 24 (2003) 1959–1967.

3. D. L. Polla, A. G. Erdman, W. P. Robbins, D. T. Markus, J. Diaz-Diaz, R. Rizq, Y. Nam, H.T. Brickner, P. Krulevitch, and A. Wang, "Microdevices in Medicine," Annual Review of Biomedical engineering, Vol. *2,2000,* pp. *552-572.*

4. David a.l Van, Terry mc guire, Robert langer, "Small scall system for in vivo drug delivery, Nature Biotechnology, Vol 21, number 10, Oct 2003, pages 1184-1191.

5. Mingjun Zhang; Tzyh-Jong Tarn; Ning Xi, "Micro/nano-devices for controlled drug delivery", International Conference on Robotics and Automation, ICRA '04. IEEE proceedings 2004, Volume 2, Apr 26-May 1, 2004 Page(s):2068 – 2073.

6. Shawgo R.S.; Richards Grayson A.C.; Li Y.; Cima M.J., "BioMEMS for drug delivery", Current Opinion in Solid State & Materials Science, Volume 6, Number 4, August 2002, pp. 329-334(6).

7. S. Henry, D.V. McAllister, M.G. Allen, and M.R. Prausnitz, "*Microfabricated Microneedles: A Novel Approach to Transdermal Drug Delivery,* " Journal of Pharmaceutical Sciences, 87, pp. 922-925 (1998).

8. Priyanka Aggarwal; Kaler, K.V.I.S.; Badawy, W, "Design and implementation of MEMS based microneedles for biomedical applications", Electrical and Computer Engineering, 2003. IEEE CCECE 2003. Canadian Conference on Volume 3, 4-7 May 2003 Page(s):1505 - 1508 vol.3.

9. Davis SP, Landis BJ, Adams ZH, Allen MG, Prausnitz MR, "Insertion of microneedles into skin: measurement and prediction of insertion force and needle fracture force", J Biomech. 2004 Aug;37(8):1155-63.

10) http://www.apogeemems.com/medical/medical.html.

11. N.Wilke, A. Mulcahy, S.R. Ye, and A. Morrissey, "*Process Optimization and Characterization of Silicon Microneedles Fabricated by Wet Etch Technology,* " Microelectronics Journal, (June 6,2005).

12) M. Romanelli and V. Falanga, "Use of a durometer to measure the degree of skin induration in lipodermatosclerosis", J. Am. Acad. Dermatol. 1995;32(1):199-91.

13). A. Magliaro and M. Romanelli, "Skin hardness measurement in hypertrophic scars", Wounds 2003; 15(3):66-70.

Vita

Joseph Ezhil Rajan Picha Muthu was born in April 25, 1975. He received his Bachelors in Pharmacy degree from Dr.MGR Medical University in India. He worked for several years in Cadila Health Care before receiving his masters in Biomedical Engineering from Jadavpur University, India. He is a recipient of the prestigious Junior Research Fellowship (JRF) from the Indian Government. After his Masters he worked as faculty in Sathyabama Deemed University, India for couple of years to establish a new Biomedical department.

He will be graduating from the Mechanical Engineering and Mechanics department of Lehigh University with a second master's degree in Mechanical Engineering. He has already accepted an offer from McGowan Institute of Cardio Vascular Remodeling and Regeneration as a Research Specialist in Biomechanics Research.

END OF TITLE